Renewable Energy xxx (2018) 1–19

Contents lists available at ScienceDirect

Renewable Energy

journal homepage: www.elsevier.com/locate/renene

Hybrid solar-biomass combined Brayton/organic Rankine-cycle plants integrated with thermal storage: Techno-economic feasibility in selected Mediterranean areas

Antonio M. Pantaleo [a, b, c, *], Sergio M. Camporeale [d], Arianna Sorrentino [b, d], Adio Miliozzi [e], Nilay Shah [c], Christos N. Markides [b, c]

[a] Dipartimento DISAAT, Università degli Studi di Bari, Via Amendola 165/A, 70125 Bari, Italy
[b] Clean Energy Processes (CEP) Laboratory, Imperial College London, South Kensington Campus, London, SW7 2AZ, UK
[c] Centre for Process Systems Engineering (CPSE), Imperial College London, South Kensington Campus, London, SW7 2AZ, UK
[d] Dipartimento DMMM, Politecnico di Bari, Via Orabona 4, 70125 Bari, Italy
[e] Energy Technologies Department, ENEA, Casaccia Research Centre, Via Anguillarese 301, 00123 S.M. di Galeria, Rome, Italy

ARTICLE INFO

Article history:
Received 1 February 2018
Received in revised form
17 July 2018
Accepted 7 August 2018
Available online xxx

Keywords:
Biomass
Organic Rankine cycle
Concentrating solar power
Externally fired gas turbine

ABSTRACT

This paper presents a thermodynamic analysis and techno-economic assessment of a novel hybrid solar-biomass power-generation system configuration composed of an externally fired gas-turbine (EFGT) fuelled by biomass (wood chips) and a bottoming organic Rankine cycle (ORC) plant. The main novelty is related to the heat recovery from the exhaust gases of the EFGT via thermal energy storage (TES), and integration of heat from a parabolic-trough collectors (PTCs) field with molten salts as a heat-transfer fluid (HTF). The presence of a TES between the topping and bottoming cycles facilitates the flexible operation of the system, allows the system to compensate for solar energy input fluctuations, and increases capacity factor and dispatchability. A TES with two molten salt tanks (one cold at 200 °C and one hot at 370 °C) is chosen. The selected bottoming ORC is a superheated recuperative cycle suitable for heat conversion in the operating temperature range of the TES. The whole system is modelled by means of a Python-based software code, and three locations in the Mediterranean area are assumed in order to perform energy-yield analyses: Marseille in France, Priolo Gargallo in Italy and Rabat in Morocco. In each case, the thermal storage that minimizes the levelized cost of energy (LCE) is selected on the basis of the estimated solar radiation and CSP size. The results of the thermodynamic simulations, capital and operational costs assessments and subsidies (feed-in tariffs for biomass and solar electricity available in the Italian framework), allow estimating the global energy conversion efficiency and the investment profitability in the three locations. Sensitivity analyses of the biomass costs, size of PTCs, feed-in tariff and share of cogenerated heat delivered to the load are also performed. The results show that the high investment costs of the CSP section in the proposed size range and hybridization configuration allow investment profitability only in the presence of a dedicated subsidy framework such as the one available in the Italian energy market. In particular, the LCE of the proposed system is around 140 Eur/MWh (with the option to discharge the cogenerated heat) and the IRR is around 15%, based on the Italian electricity subsidy tariffs. The recovery of otherwise discharged heat to match thermal energy demand can significantly increase the investment profitability and compensate the high investment costs of the proposed technology.

1. Introduction

The increased utilization of renewable energy for the displacement of fossil-fuel consumption is an essential component of the transition to a low-carbon, sustainable energy future [76,77] and at the centre of the European Commission's 2030 energy strategy [1].

* Corresponding author. Dipartimento DISAAT, Università degli Studi di Bari, Via Amendola 165/A, 70125 Bari, Italy.
E-mail addresses: antonio.pantaleo@uniba.it, a.pantaleo@imperial.ac.uk (A.M. Pantaleo).

https://doi.org/10.1016/j.renene.2018.08.022

Solar and biomass are among the most widespread and promising renewable energy sources, however, solar energy is inherently intermittent and needs to be integrated with energy storage and programmable generation systems in order to match energy demand.

1.1. Literature review on hybrid solar-biomass and combined-cyle power plants

A hybrid Brayton solar/gas-fired plant in which a constant power output is ensured by natural-gas combustors was proposed in Ref. [2]. In this context, biomass can be an interesting alternative for compensating the fluctuations of solar energy. On the other hand, the necessity of a constant and reliable supply of biomass at an affordable price is one of the biggest challenges for the development of biomass power plants [3]. Hybridization of solar thermal with biomass combines two energy sources that complement one each other, both seasonally and diurnally [4]. Specifically, Hussain et al. [5] demonstrated that hybrid concentrating solar (CSP) and biomass power plants are technically viable alternatives to conventional fossil-fuelled plants. San Miguel at al. [6] used the life cycle assessment to highlight the environmental benefits of CSP hybridization by means of biofuels, instead of natural gas, including the environmental balances of biofuel production and transportation. The thermodynamic potential and a comparison of different types of solar-thermal collectors in the context of solar power-generation and cogeneration applications is considered in Ref. [78], where it is reported that the type of collector is strongly influenced by the characteristics of the solar resource. Parabolic trough collectors (PTCs) were found to be well suited to regions with good direct-solar irradiance conditions, but less so when diffuse irradiation accounts for a significant fraction of the total solar resource. Therefore they are considered good options for hybridization, as they have good summer performance but poor performance at low solar radiation levels, therefore offering promising options for integration with biomass energy during winter or during the night. Mishra et al. [7] compared various PTCs technologies in a solar biomass hybrid plant to choose the optimal one to match the thermal output. Nevertheless, the thermal inertia of biomass furnaces makes this technology suitable for base load operation but not for load-following options to meet variable energy demand. The integration of thermal energy storage (TES) can compensate these solar energy fluctuations and energy demand variations to overcome the individual drawbacks of solar and biomass as primary energy resources, thus facilitating smart and flexible operation strategies [8].

Organic Rankine cycle (ORC) technology is based on the Rankine cycle but employs organic working fluids and is particularly suitable for the conversion of low-to-medium temperature heat [9] and for employment in small-to-medium scale applications [77]. Many thermodynamic and techno-economic feasibility studies on the employment of ORC technology in CHP applications have been reported in literature [10,79,80], including of working-fluid selection [11] and optimal cycle design, as well as studies specifically relating to solar applications [81,82], including with integrated TES [83,84]. Many ORC performance optimization methods have been proposed in literature. Conventional methods have been used in ORC optimization problems as in Ref. [12], where the steepest descendent method was adopted to minimize the ratio of total heat transfer areas and total net power. However, these methods are initialized in a way that can risk convergence to sub-optimal solutions. On the other hand, global optimization tools based on genetic algorithms (GAs) have been successfully adopted in heat transfer problems for their simplicity and robustness [13]. Xi et al. [14] analysed different ORC configurations with six working fluids adopting GA to maximize exergy efficiency, while Wang et al. [15] examined the effects of some thermodynamic design parameters on the power output and heat exchanger areas. Other ORC optimization problems have been solved by means of gradient-based methods [16], where a hybrid solar-biomass plant supplies heat to the ORC plant.

The performance of hybrid solar-biomass plant configurations under a variable solar input was studied by Srinivas & Reddy [17], who simulated a solar-biomass regenerative steam-Rankine cycle without TES, while Vidal & Martin [18] proposed the integration of biomass gasification in a CSP facility. In this case, the options of using syngas for hydrogen production and heat generation in a furnace, vs power generation in an open Brayton-cycle were compared, with the biomass section coupled to a tower-based CSP plant and a molten salt (MS) used as the heat transfer fluid (HTF). A general multi-criterion approach for selecting the most suitable CSP technology for hybridization with Rankine power plants using conventional (gas, coal) and alternative (biomass, wastes) fuels was suggested by Peterseim et al. [19], including key factors such as technology maturity, environmental impact, economics and site-specific solar yield. In Ref. [20], the same authors proposed a method for classifying CSP hybridization depending on the interconnections of the plant components, and including biomass, fossil fuel and geothermal sources. Other hybrid solar-biomass configurations are based on PTCs, backup boilers and Rankine cycles [21] using thermal oil as HTF [22] or MSs [23], the substitution of steam bleed regeneration with water preheating by solar energy [24] or Fresnel collectors [25] to increase temperatures. Some applications of CSP plants combined with gas turbines consider the use of solar towers or solar dishes with compressed air as HTF in internally fired cycle configurations [26]. More recently, Bai et al. [27] simulated a solar-biomass power generation system integrating a two-stage gasifier using two different types of solar collectors applied to drive thermochemical pyrolysis and gasification processes. In another study of interest, a mini hybrid CSP plant combining concentrating solar energy and biomass to drive an ORC was considered [28], in which PTCs were coupled to a biogas boiler used as backup. The results reported an improved annualized global electric efficiency with hybridization (from 3.4% to 9.6%). Integration of a PTC-based CSP to a CHP steam turbine was reported in Ref. [29], where a steam turbine plant was fed by sugarcane bagasse. Solar integration was considered for displacing the high-pressure steam extraction of a condensing-extraction steam turbine via feedwater preheating; operation in a fuel-economy mode was employed to save bagasse during the harvesting period with use of the economized bagasse off-season. In this case, the hybridization of CSP with biomass allowed base-load generation, while solar thermal input facilitated the rational use of seasonal bagasse.

The use of biomass has been widely investigated in the literature as it provides added socio-economic and environmental benefits, especially when the organic by-products are also utilized [30]. In the case of small-to-medium scale CHP plants, this includes dual-fuelling of biomass and natural gas in externally/internally-fired gas turbines [31]. Applications in the tertiary and industrial sectors have been investigated in Ref. [32], while residential end-users have been analysed in Ref. [33]. The influence of part-load performance on optimal EFGT operation was investigated in Ref. [34], while the improved energy performance and profitability of bottoming ORCs has been investigated in different energy-demand segments from technical [35,80] and exergoeconomic [36] points of view. The literature on ORC systems and working-fluid selection for waste-heat recovery is also extensive [37]. Oyewunmi et al. [38,39] analysed the effect of working-fluid mixtures on the efficiency and power output of ORC systems by using the molecular-

Please cite this article in press as: A.M. Pantaleo, et al., Hybrid solar-biomass combined Brayton/organic Rankine-cycle plants integrated with thermal storage: Techno-economic feasibility in selected Mediterranean areas, Renewable Energy (2018), https://doi.org/10.1016/j.renene.2018.08.022

based statistical associating fluid theory (SAFT), specifically, the SAFT-VR Mie equation of state for the prediction of the working-fluid properties (The interested reader can also refer to extensions of these approaches to a group-contribution version of SAFT referred to as SAFT-γ Mie [85,86], which can be used for simultaneous working-fluid design and overall ORC system performance optimization). Economic analyses have also been performed by the same authors, in Ref. [40] in relation to the use of working-fluid mixtures, and in Ref. [87] in relation to supercritical cycles. More recently, Pratticò et al. [41] investigated a small solar-powered ORC plant in a rural application with a focus on optimizing the heat-source temperature, while a combined cycle with a 1.3 MW biomass EFGT topping cycle and 0.7 MW bottoming ORC plant was proposed in Ref. [42]. Furthermore, previous research from the same authors has addressed the integration of PTCs and molten salt TES with biomass combustion in externally fired gas turbines (EFGT) [43], estimating the profitability of such hybridization options in the Italian energy policy framework.

1.2. Contents of innovation of the proposed plant

This paper progresses beyond the hybrid EFGT + ORC system proposed in Ref. [43], presenting a novel CHP plant based on independent “power blocks” (PBs), which comprise: electric power generation (gas turbine and ORC), thermal energy sources (biomass furnace and CSP plant), and energy storage (a thermal storage as depicted in Fig. 1). The proposed configuration is characterized by a high degree of flexibility and can be integrated to additional (and different) power blocks such as gen-sets, electric energy storage (electric batteries), wind turbines or photovoltaic modules. The main novelty is the connection of thermal sources (exhaust gas from the topping cycle and from the CSP) and thermal sinks (bottoming ORC and thermal users) to the TES that can compensate the fluctuations of the solar input as well as electricity and/or heat demand.

Several TES typologies can be used to recover heat from relatively high temperature: a critical review of technologies and materials is proposed in Ref. [44]. In this work, considering the range of temperatures available from EFGT and PTC [44], the two-tank technology that uses MSs as HTF and heat storage medium has been selected. This technology, referred as 'sensible heat storage' with direct heating, has the advantage of a relatively low-cost medium for storage and fluid vector, and indirect heating arrangements that need additional heat exchangers for charge and discharge of the thermal storage. Even if low cost material is chosen, the size of the TES needs to be optimized to minimize exergy losses when heat is recovered from the thermal sources to the storage and when the heat extracted from the storage is transferred to the bottoming thermal sinks.

The selected MSs mixture determines the operating range of the TES. The minimum temperature at which the MS mixture remains liquid in the cold tank determines the minimum temperature of heat storage.

The novelty of the proposed plant scheme relies on the hybrid combined configuration that offers promising opportunities for flexible operational strategies and coupling of solar and biomass sections. In particular, the adoption of a combined cycle with a biomass fired EFGT and a bottoming ORC that is fed by solar energy and heat discharged from the topping turbine, potentially allows an independent operation of the system with only one of the two sources, which could occur in case of low solar radiation, high biomass costs or modulation of the electric output for load following. Moreover, the high temperature of the cogenerated heat allows matching on site thermal energy demand or coupling to another ORC that can operate at lower temperature, so increasing the electric efficiency or flexibility of the heat/electricity output.

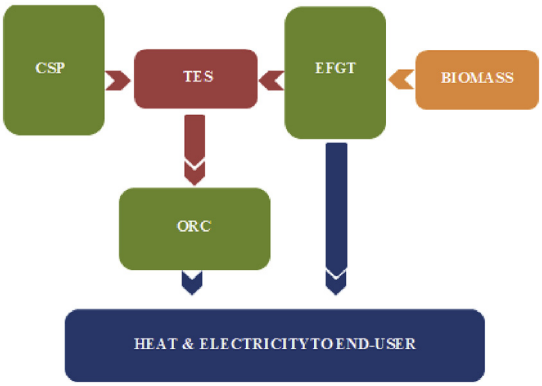

Fig. 1. Power blocks and energy flows through the proposed plant.

The paper is structured as follows: in the second section, the thermodynamic description of the topping EFGT, bottoming ORC and of the solar plant, including the TES, is provided, and the simulation model adopted to predict the performance of the solar system connected to the TES is also described; in Section 3, energy and exergy balances of the system at design condition are reported; in Section 4 the energy yield analysis in different plant locations and thermal storage size is presented; in section 5 the costs assessment and the hypotheses for the economic analysis are presented, while the results are reported in Section 6 and the conclusions are drawn in Section 7.

2. Plant description

In this section, the combined-cycle system components are described. Fig. 2 shows the plant layout of the three blocks that compose the proposed configuration and which are detailed hereafter.

2.1. Biomass EFGT section

The topping cycle is a biomass-fired EFGT (Fig. 2(a)). The thermodynamic cycle is characterized by an inter-refrigerated compression (A-C) with overall pressure ratio of 10; a gas-gas heat exchanger (High Temperature Heat Exchanger, HTHE) transfers the heat of the flue gas exiting the biomass furnace to the compressed air (C-D) that is heated to a turbine inlet temperature (TIT) of 800 °C. This relatively low temperature is chosen to keep low the cost of heat exchanger that can be made of steel. The air is then expanded in the turboexpander (D-E): the turbine outlet temperature is 390 °C. The heat of the air exiting the turbine is recovered and transmitted to the molten salts flowing in the heat exchanger indicated as Heat Recovery Molten Salts Heat Exchanger (HRMSHE) in Fig. 2(a). Since the minimum temperature of the cold tank is 200 °C, sensible heat can be further recovered from the gas for cogeneration. The thermodynamic cycle is represented by mean of a Temperature-entropy diagram, shown in Fig. 3.

The air in the biomass combustion is taken directly from the ambient. Since the two gas circuits (circuit of the working air flowing into the turbine and circuit of the combustion air flowing into the furnace) are decoupled, the proposed scheme allows a flexible regulation of the air-to-fuel ratio, taking into account the furnace characteristics, the lower heating value of the biomass, its moisture content, etc. It is also possible to have a partial flue gas recirculation, in order to lower the temperature of the hot gas

Please cite this article in press as: A.M. Pantaleo, et al., Hybrid solar-biomass combined Brayton/organic Rankine-cycle plants integrated with thermal storage: Techno-economic feasibility in selected Mediterranean areas, Renewable Energy (2018), https://doi.org/10.1016/j.renene.2018.08.022

entering the HTHE and avoid that high metal temperatures deteriorate the molecular structure of the MSs.

2.2. CSP and TES sections

The solar collectors are based on the ENEA technologies of PTCs largely described in Refs. [45–47], while a numerical simulation of the PTC performance is proposed in Ref. [48]. The main characteristic is the use of MSs as HTF instead of synthetic oil. This presents two main advantages: lower environmental impact and fire risks and higher maximum temperature that can be raised up to about 500 °C. The main drawback of MSs is the risk of freezing that occurs at about 120 °C; however, they can be considered liquid only at temperatures higher than 200 °C [49]. A mixture of MSs (lithium, sodium and potassium nitrates) is chosen for both the HTF and the TES medium. This scheme is generally referred as "Direct Heating" TES [50] because it does not need a heat exchanger to transfer heat from the solar plant to the thermal storage, so avoiding the related costs. MSs flow in the solar collectors during the day but also at night, because continuous recirculation can avoid freezing in the circuit. However, heat losses from the solar collectors are generally low at night. In the event of a lack of heating from the sun, the temperature can be restored using some heaters inside the two tanks.

Minimum and maximum temperatures of the PTC are therefore equal to those of the TES: the max temperature is limited to 370 °C, in order to recover heat from the EFGT while the min temperature cannot be lower than 200 °C to avoid risk of freezing for the molten

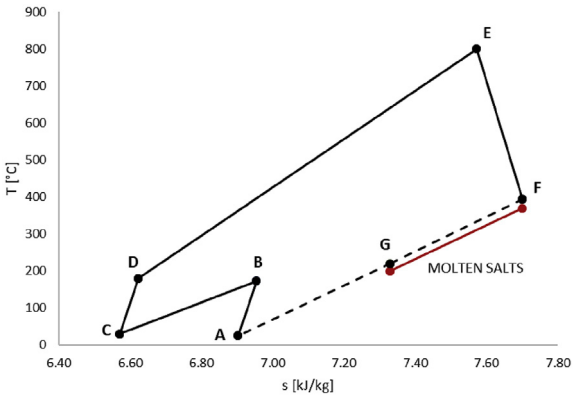

Fig. 3. T-s diagram of the EFGT plant.

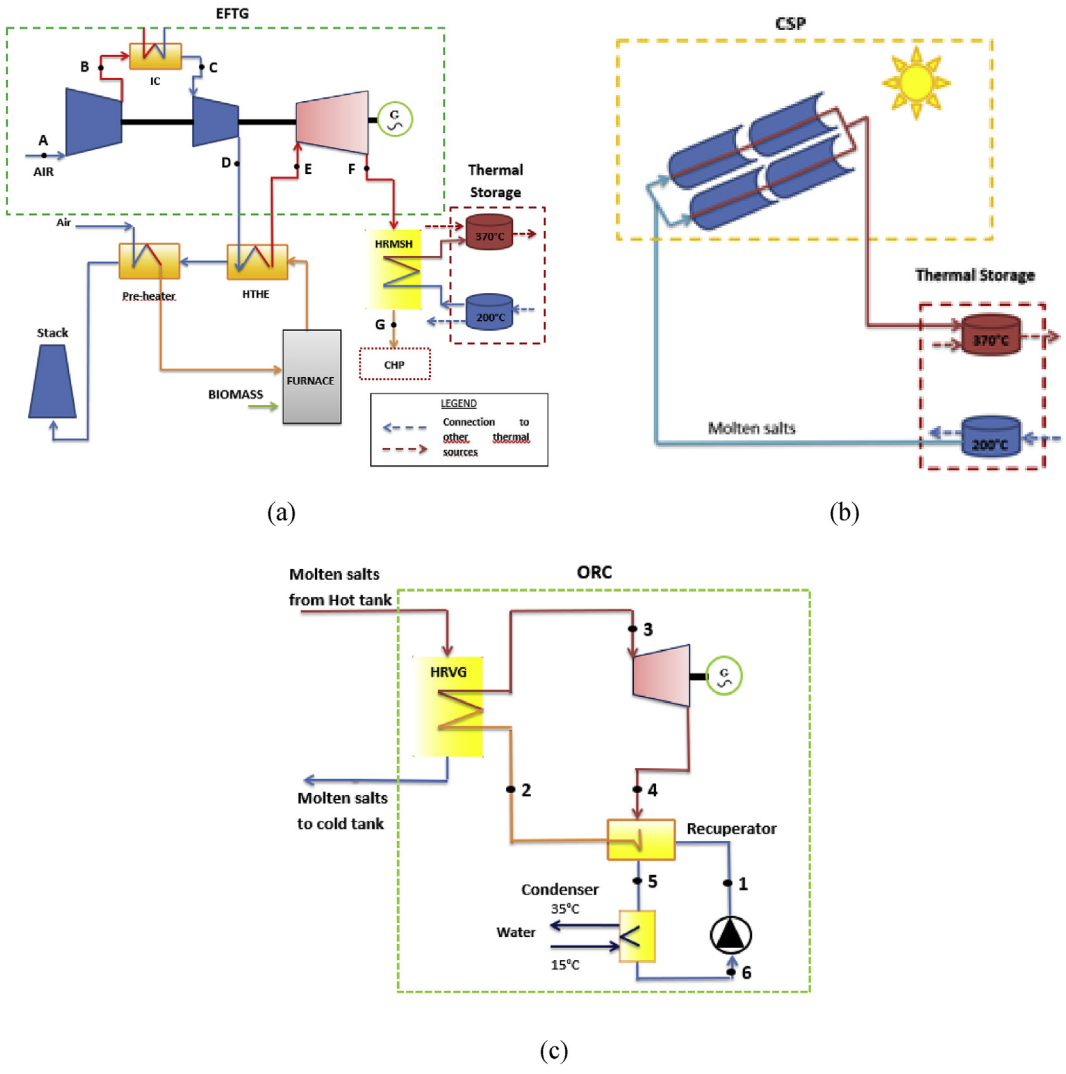

Fig. 2. Layout of the power blocks that compose the plant: (a) EFGT; (b) CSP with TES; (c) ORC plant.

Please cite this article in press as: A.M. Pantaleo, et al., Hybrid solar-biomass combined Brayton/organic Rankine-cycle plants integrated with thermal storage: Techno-economic feasibility in selected Mediterranean areas, Renewable Energy (2018), https://doi.org/10.1016/j.renene.2018.08.022

salts.

The CSP consists of one or more lines of collectors in a cascade configuration: the number of collectors of each line is evaluated to raise the temperature of the salts flowing in the receiver from 200 to 370 °C, with a standard direct normal irradiance (DNI) of 800 W/m^2 [51]. The solar collectors considered in this work have been lengthily tested in the ENEA facilities [52], and are characterized by a width of 5.9 m and a length of 12 m that determines a useful intercepting area of 67.3 m^2, equal to the 95% of the geometric area. The collectors are controlled by a central driving unit and form a Solar Collector Assembly (SCA). A single SCA includes eight collectors for a total length of 96 m. The collector axis is supposed to have a N-S orientation and an E-W track axis. Within such hypotheses, the average photo-thermal efficiency of the solar collectors is $\eta_{sol,\ PTC} = 73\%$ which includes a cleaning efficiency of 95% and a solar field availability of 99%. For each collector line, considering the cross section of the receiver and assuming a fluid velocity of 1.2 m/s, a MS flow rate of 6 kg/s is obtained and the overall length is 506 m. This means that each line is composed by 6 collectors of 96 m, with an intercepted area of about 3230 m^2 per each line and thermal power output of 1.885 MW. The results of the design of the solar collectors' line are summarized in Table 1.

Considering the scheme of Fig. 2, the share of energy input (solar/biomass) can be chosen considering the local availability of biomass and solar energy.

2.3. ORC section

The bottoming ORC recovers heat from MSs flowing from the Hot Tank to the Cold Tank of the TES as shown in Fig. 2(c). Since the heat is available at high temperature (from 370 to 200 °C) a recuperative configuration with superheating is chosen for the organic cycle. A pump (6–1) compresses the fluid up to the evaporating pressure and supplies it to the recuperator (1–2) that preheats the working fluid. Heat is supplied to the ORC plant in a heat exchanger between MSs and organic fluid heat recovery Vapour Generator (HRVG) (2–3) and then electric power is produced by the expansion of the organic fluid in the turbine (3–4). Finally, the hot organic vapour exiting from the turbine preheats the fluid entering in the recuperator (4–5) and condenses in a water condenser (5–6) until the inlet pump conditions. Selection of the working fluid is a crucial aspect in ORC analysis. Dry fluids, with a positive slope of the saturation curve in the *T-s* diagram, show a better thermal efficiency [53] with respect to other working fluids. Among dry fluids, Toluene is chosen because it shows a relatively high critical temperature and good performance at temperature ranges higher than 300 °C [54]. Moreover, Toluene has good environmental and safety properties, with both ozone depletion potential (ODP) and global warming potential (GWP) equal to zero.

The ORC parameters have been designed in order to meet the operating conditions of the MSs. A single-objective genetic algorithms (GA) based optimization is performed, to maximize the thermal efficiency of the cycle. A GA procedure starts from a randomly initial population that through genetic operators and stochastic selection, mutation and crossover, generates other populations by combining the best individuals [13]. The process ends when the global optimal value of the objective function is found. GAs involve a search from a population of solutions and not from a single point, hence convergence to sub-optimal solutions is prevented.

An in-house code in Phytoon language has been adopted for the parametric single-objective optimization process. In the code, a set of equations have been implemented to model each ORC component. The thermodynamic properties of the organic fluid have been evaluated by means of Coolprop library [55]. The objective function was the ORC thermal efficiency maximization:

$$\eta_{ORC} = \dot{W}_{exp} - \frac{\dot{W}_{pump}}{\dot{Q}_{ORC,in}}, \quad (1)$$

where $\dot{W}_{exp}$ and $\dot{W}_{pump}$ are the expander output power and pump input power, and $\dot{Q}_{in}$ is the thermal input of the molten salt stream coming from the Hot Tank (370 °C) and the returning temperature to the Cold Tank (200 °C). In this study, the evaporating pressure P_{ev}, the turbine inlet temperature T_{TIT} and the pinch point temperature difference (ΔT_{pp}) in the HRVG are considered as optimization parameters. The optimization problem has been solved under the following constraints: $0.4P_c \leq P_{ev} \leq 0.9P_c$, where P_c is the critical pressure of Toluene; $T_{TIT} < T_{HOTTANK}$; $7\ K \leq \Delta T_{PP} \leq 10\ K$; minimum temperature difference in the RHE recuperator, $\Delta T_{min,\ RHE} \geq 5K$. Only subcritical cycles have been considered. Further thermodynamic assumptions for the ORC cycle are summarized in Table 2.

The convergence in the single-objective optimization problem was reached after 13 generations, each generation made by 200 individuals. The *T-s* diagram of the cycle is shown in Fig. 4 where

Table 1
Performance of a single line of solar collectors under rated conditions.

Description	Value
Intercepting area (m^2)	3230
Ground area (m^2)	8075
Overall photo-thermal efficiency	0.73
Thermal power output (MW)	1.885

Table 2
Basic calculation hypotheses for the ORC plant.

Description	Value
Pump isentropic efficiency	0.75
Pump mechanical efficiency	0.96
Turbine isentropic efficiency	0.80
Turbine mechanical efficiency	0.96
Electric generator efficiency	0.95
Condenser temperature	40 °C

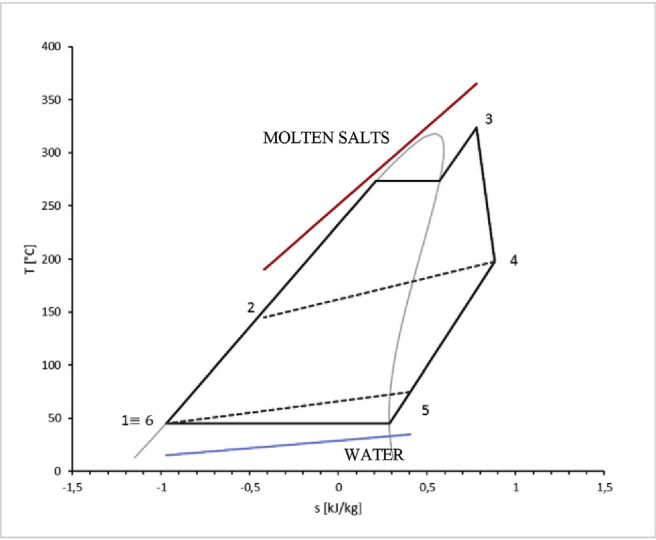

Fig. 4. T-s diagram of the ORC plant obtained from the optimization.

Please cite this article in press as: A.M. Pantaleo, et al., Hybrid solar-biomass combined Brayton/organic Rankine-cycle plants integrated with thermal storage: Techno-economic feasibility in selected Mediterranean areas, Renewable Energy (2018), https://doi.org/10.1016/j.renene.2018.08.022

Table 3
Results of the optimization process.

Description	Value
Evaporating pressure	21.7 bar
Turbine inlet temperature	322 °C
Pinch point temperature difference in HRVG	7.06
Cycle thermal efficiency	30.4%

the red line represents MSs temperature profile while the blue line represents the cooling water temperature profile, respectively. Results are summarized in Table 3.

Under the optimal set of operating conditions, the cycle thermal efficiency results equal to 30.4% and the ORC electric efficiency is $\eta_{el,\,orc} = 29\%$, considering electric generator efficiency. The state points in Fig. 4 are correspondent to the state points in Fig. 2 (c).

3. Design-point performance

This section analyses the design point performance of the plant. Considering the scheme of Fig. 2, the share of biomass and solar energy inputs can be chosen considering the resources local availability. The aim of this section is to determine the rated power for the different plant components and to set properly the overall solar field size. For a better understanding of the energy conversion process, a first law energy analysis is firstly carried out; then, an exergy analysis is carried out in order to detect the main causes of irreversibility for the plant and to suggest the most profitable modifications to improve the energy conversion efficiency.

3.1. First law analysis at the design point

Let's consider first the EFGT including the biomass furnace Fig. 2(a). The rated lower heating value (LHV) input produced by the biomass combustion is:

$$\dot{E}_{biom} = \dot{m}_{biom} LHV_{biom}, \tag{2}$$

where $\dot{m}_{biom}$ is the biomass flow and LHV_{biom} is lower heating value of the biomass equal to 4.18 kWh/kg. The biomass combustion energy is partially transmitted to the compressed air flowing in the HTHE. The biomass furnace efficiency is expressed by:

$$\eta_{fur} = \frac{\dot{Q}_{HTHE}}{\dot{E}_{biom}}. \tag{3}$$

This efficiency is about 79,6% due to the relatively high energy losses for sensible heat of the exhaust gas and unburnt fraction of the biomass.

The net electric power output of the EFGT is:

$$\dot{W}_{net,EFGT} = \eta_{gen,el}\left(\dot{W}_t - \dot{W}_{c,I} - \dot{W}_{c,II}\right), \tag{4}$$

where $\eta_{gen,el}$ is the electric generator efficiency, $\dot{W}_t$ is the turbine power output, $\dot{W}_{c,I}$ and $\dot{W}_{c,II}$ are respectively the power input of first and second compressor stages. The available heat flow at the turbine exit $\dot{Q}_{av}$ is the heat flow that could be recovered when the gas is cooled to the ambient temperature. Therefore $\dot{Q}_{av}$ can be evaluated from the gas temperature at the turbine exit T_F and the ambient temperature T_{amb} from:

$$\dot{Q}_{av} = \dot{m}_g\, c_{p,g}(T_F - T_{amb}), \tag{5}$$

where $\dot{m}_g$ and $c_{p,g}$ are the mass flow and specific heat at constant pressure of the air working in the turbine, respectively. The heat of the air exiting the turbine is recovered in the HRMSHE (Fig. 2(a)) and transferred to the MSs to supply heat to the TES. The thermal flow $\dot{Q}_{rec}$ that can be recovered in the HRMSHE is determined by the MS temperature in the Cold Tank. Considering a Cold Tank temperature $T_{COLD\ TANK} = 200\,°C$, and assuming $\Delta T_{min} = 20°C$ between hot and cold fluids at the cold end of the HRMSHE, the temperature of the gas exiting the heat exchanger results $T_G = 220°C$ and the heat flow recovered is

$$\dot{Q}_{rec} = \dot{m}_g\, c_{p,g}(T_F - T_G). \tag{6}$$

We will assume that, at the design point, the heat flow $\dot{Q}_{rec}$ will be entirely delivered to the bottoming ORC cycle and no thermal energy will be stored or discharged. Further heat can be recovered from the air exiting the HRMSHE at the temperature $T_G = 220\,°C$ and used to serve on site heating demand.

We consider the additional solar contribution to the thermal input of the ORC Power Block (ORC_PB). It is worth noting that in the proposed scheme the share of the solar input can be varied in relation to the local disposability of the energy sources, solar and biomass. The total thermal input to the ORC at design condition is:

$$\dot{Q}_{orc,in} = \dot{Q}_{rec} + \dot{Q}_{th,sol,ORC\_PB}, \tag{7}$$

where $\dot{Q}_{th,sol,ORC\_PB}$ is the additional thermal power delivered to the ORC power block produced by solar plant. Then let's consider the solar multiple (SM) of the solar plant. Considering a design point value for the Direct Normal Irradiance (DNI), the thermal power generated by the solar field at the design point, $\dot{Q}_{th,solar\_field}$, is related to the total intercepting area A_c and the efficiency $\eta_{sol,\,PTC}$ of the solar collectors that compose the solar field by:

$$\dot{Q}_{th,solar\_field} = \eta_{sol,\,PTC} \cdot A_c \cdot DNI. \tag{8}$$

The Solar Multiple (SM) is the ratio of the thermal power generated by the solar field at the design point, $\dot{Q}_{th,solar\_field}$, to the thermal power input of the power block at reference condition $\dot{Q}_{th,sol,ORC\_PB}$:

$$SM = \frac{\dot{Q}_{th,solar\_field}}{\dot{Q}_{th,sol,ORC\_PB}}. \tag{9}$$

Therefore, the SM is a measure of the excess thermal power produced by the solar field at the design point that cannot be absorbed by the power block and should be delivered to the TES. Therefore, the thermal power delivered to the TES at the design point is:

$$\dot{Q}_{th,TES} = \dot{Q}_{th,solar\_field} - \dot{Q}_{th,sol,ORC\_PB}. \tag{10}$$

According to these assumptions, at the design point with biomass + solar input contribution, the combined cycle net power output is:

$$\dot{W}_{el,tot} = \dot{W}_{net,\,EFGT} + \dot{W}_{net,\,ORC}. \tag{11}$$

The net electric efficiency is the ratio of the produced electric power $\dot{W}_{el,\,tot}$ and the sum of biomass and solar input power:

Please cite this article in press as: A.M. Pantaleo, et al., Hybrid solar-biomass combined Brayton/organic Rankine-cycle plants integrated with thermal storage: Techno-economic feasibility in selected Mediterranean areas, Renewable Energy (2018), https://doi.org/10.1016/j.renene.2018.08.022

$$\eta_{el} = \frac{\dot{W}_{el,\,tot}}{\dot{E}_{biom} + \dot{E}_{sol}}, \tag{12}$$

where $\dot{E}_{sol}$ is the input of solar energy, evaluated from the part of the solar thermal power delivered to the ORC power block:

$$\dot{E}_{sol} = \frac{\dot{Q}_{th,\,sol,ORC\_PB}}{\eta_{sol,\,PTC}} = A_r \cdot DNI. \tag{13}$$

where A_r is the reference area related to the part of the solar thermal power delivered to the ORC. It is worthwhile to show that $SM = A_c/A_r$.

The energy balance of the whole plant is reported in the energy flow scheme in Fig. 5. As far as concerns the biomass input, the same EFGT proposed in Ref. [42] with a thermal power input $\dot{E}_{biom} = 9050\ kW$.The thermal input to the gas cycle is given by the heat flux in the HTHE, $\dot{Q}_{HTHE} = 7201\ kW$, with a relatively low efficiency of the furnace due to the sensible heat of the exhaust gas. Based on the hypotheses detailed in Ref. [42], the net power output of the EFGT, calculated from Eq. (5), is $\dot{W}_{net,EFGT} = 1388$ kW while $\dot{Q}_{av}$ is calculated from Eq. (6) results equal to 4043 kW.

The heat flow $\dot{Q}_{av}$ is partly recovered and transferred to the MSs flowing in the HRMSHE. The heat flow recovered is $\dot{Q}_{rec} = 1890$ kW. At the design point, we assume that such heat flow is entirely transferred to the ORC power block and does not contribute to the energy storage.

We revert now to the solar plant. In this work, it has been also assumed that the additional contribution of the solar field will be the 30% of the total rated thermal input to the ORC power block, corresponding to a thermal power $\dot{Q}_{th,sol,ORC_PB} = 900$ kW. The total input to the ORC resulting from Eq. (7) is hence $\dot{Q}_{orc,in} = 2780$ kW while, considering $\eta_{el,\,orc}$ of the optimal cycle, the electric power output $\dot{W}_{net,\,ORC}$ is 800 kW.

Let's then consider the solar field assuming, at the design point, a DNI of 800 W/m^2. Under such conditions, a single line of solar collectors generates a thermal power output of 1.885 MW. Then, considering the thermal power delivered to the power block, $\dot{Q}_{th,sol,ORC_PB} = 0.900$ MW, the we can reasonably examine two scenarios:

- Scenario no. 1: 1 line of solar collectors, SM = 1.885MW/0.900 MW = 2.1
- Scenario no. 2: 2 lines of solar collectors, SM = 2 · 1.885MW/0.900 MW = 4.2

Fig. 5 shows the scenario with SM = 2.1. In such case, from Eq. (7), the excess heat produced by the solar field and delivered to the TES is $\dot{Q}_{th,TES} = 985$ kW. The overall plant net electric power output results $\dot{W}_{el,tot} = \dot{W}_{net,\,EFGT} + \dot{W}_{net,\,ORC} = 2188$ kWe while the thermal power output available for cogeneration is $\dot{Q}_{cog} = 2152$ kWt at 220 °C. In the case of no solar contribution [42] and with a direct heat recovery of the heat available $\dot{Q}_{av}$ from EFGT,$\dot{Q}'_{orc,in} = 2413$ kW the gas can be cooled to 104 °C. Consequently the $\dot{W}'_{net,\,ORC}$ results 700 kW and the total electric power output is $\dot{W}'_{el,\,tot} = 2083$ kWe and the thermal power output for cogeneration is of 963 kWt. The modelling results report a net electric efficiency of 21.5% for the 100% biomass case.

3.2. Second law analysis

The main limit of the energy analysis is that it does not provide information about irreversibility of the system. Exergy (or "second law") analysis, which is based on the second law of thermodynamics [56], provides information on inefficiency of the different processes in order to identify components that cause the largest exergy losses.

Exergy is the maximum work we can obtain from a fluid until it reaches the "dead-state" condition ($T_0 = 298.15$ K, $P_0 = 1$ atm = 1.01325 bar). Unlike energy, exergy is not conservative. Exergy per unit mass can evaluated as the sum of a "physical" and a "chemical" component [57]:

$$e_x = e_x^{ph} - e_x^{ch}. \tag{14}$$

"Physical exergy" (e_x^{ph}) gives the potential work that could be obtained from the fluid due to its thermodynamic state (temperature and pressure) and can be calculated from:

$$e_x^{ph} = h - h_0 - T_0(s - s_0), \tag{15}$$

where h and s represent enthalpy and entropy of the fluid at the considered state point and at the dead-state, respectively. In the present work, the mechanical terms corresponding to kinetic and

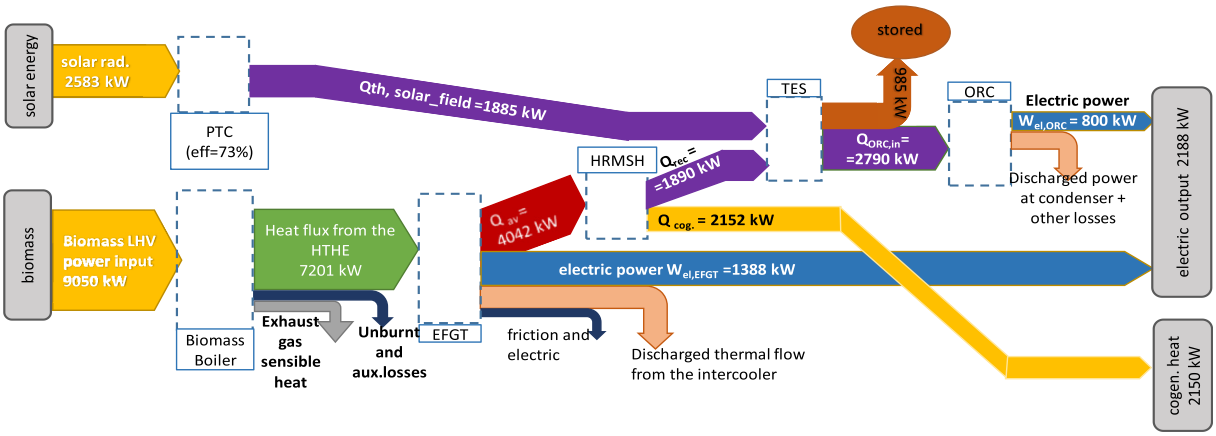

Fig. 5. Energy flows at the design point.

Please cite this article in press as: A.M. Pantaleo, et al., Hybrid solar-biomass combined Brayton/organic Rankine-cycle plants integrated with thermal storage: Techno-economic feasibility in selected Mediterranean areas, Renewable Energy (2018), https://doi.org/10.1016/j.renene.2018.08.022

Table 4
Exergy accounting for the plant components.

Component	Exergy input	Exergy output	Exergy destroyed
EFGT	Biomass $\dot{E}_x^{biom} = 9593$ kW	Mechanical power output $\dot{W}_{EFGT} = 1623$ kW Thermal exergy to molten salts circui $\dot{E}_x^Q = 8938$ *kW* Thermal exergy for cogeneration $\dot{E}_x^Q = 98.1$ *kW*	$\dot{I} = 6978$ *kW*
Solar collectors	Solar irradiance $\dot{E}_x^{rad} = 1149.2$ kW	Thermal exergy to molten salts circuit $\dot{E}_x^Q = 484.5$ *kW*	$\dot{I} = 664.7$*kW*
Molten salts circuit	Thermal exergy $\dot{E}_x^Q = 893.8$ kW (from EFGT) $\dot{E}_x^Q = 484.5$ kW (from solar collectors)	Thermal exergy to ORC $\dot{E}_x^Q = 1270$ kW	$\dot{I} = 1083$ *kW*
ORC	Thermal exergy $\dot{E}_x^Q = 1270$kW	Mechanical power output $\dot{W}_{ORC} = 846.5$ kW	$\dot{I} = 4235$ *kW*

gravity potential energy will be neglected. "Chemical exergy" (e_x^{ch}) is a function of the material stream composition; for a gas mixture, supposed ideal, it can be calculated as [58]

$$e_x^{ch} = \sum_{j=1}^{N} x_i \cdot e_{x,j}^{ch,0} + R\,T_0 \sum_{j=1}^{N} x_j \ln x_j, \tag{16}$$

where x_j and $e_{x,j}^{ch,0}$ are mole fraction and standard chemical exergy of substance j that compose the stream, respectively, evaluated at the dead state. The chemical exergy can be evaluated from the standard Gibbs free energy as shown in Ref. [59] that gives also the values for several substances. For the biomass, the physical exergy can be neglected since the biomass is delivered to the furnace at ambient conditions while the chemical exergy can be evaluated from its lower heating value (LHV) from:

$$e_{x,biom}^{ch} = \beta \cdot LHV_{biom}, \tag{17}$$

where the coefficient β can be evaluated from the chemical composition of the biomass [60]. Here, we assume $\beta = 1.02$.

Considering steady-state conditions, for every component of the plant, a control volume can be defined in order to identify mass, work and heat flows that cross the volume. The exergy balance can be expressed as:

$$\sum_{in} \dot{m} \cdot e_x + \dot{E}_x^Q = \sum_{out} \dot{m} \cdot e_x + \dot{W}_{act} + \dot{I}, \tag{18}$$

where $\dot{E}_x^Q$ is the net exergy transfer rate associated with the heat transfer flows $\dot{Q}_i$ from heat sources at temperature T_i placed in the surroundings:

$$\dot{E}_x^Q = \sum_{i=1}^{N} \dot{Q}_i \left(1 - \frac{T_0}{T_i}\right), \tag{19}$$

$\dot{W}_{act}$ is the actual rate of work produced by the component and $\dot{I} = T_0 \dot{S}_{\mathrm{gen}}$ is the "irreversibility" or the rate of work lost due to the entropy rate generated, $\dot{S}_{gen}$, due to the irreversibility within the control volume as well as those associated to the irreversible heat transfer with the heat sources.

For the solar field we consider the radiation $\dot{E}_{\mathrm{sol}} = A_r \cdot DNI$ intercepted by the reference area A_r (see Eq. (13)). The maximum useful work rate available from radiation, $\dot{E}_x^{rad}$ can be calculated from Petela's formula:

$$\dot{E}_x^{\mathrm{rad}} = A_r\, DNI \left(1 - \frac{T_0}{T_{\mathrm{sol}}}\right), \tag{20}$$

where T_{sol} is the solar temperature (4350 K) which is approximately 3/4 of the blackbody temperature of sun. The thermal exergy transferred from the receiver to the working fluid due to the incident radiation can be expressed as:

$$\dot{E}_{x,sol}^Q = \eta_{\mathrm{sol,\ PTC}} \dot{A}_r\, DNI \left(1 - \frac{T_0}{T_{lm}}\right), \tag{21}$$

where T_{lm} is the log-mean temperature of inlet and outlet molten salt stream flowing in the receiver. It is worth to recall here that the inlet temperature of the molten salts is the temperature of cold tank and the outlet temperature should be equal to that of the hot tank.

Considering the overall plant, there are two exergy inputs: the solar exergy input is $\dot{E}_x^{\mathrm{rad}}$ given by Eq. (20) while the biomass exergy input $\dot{E}_x^{biom}$ is related to mass flow rate of biomass $\dot{m}_{biom}$ by:

$$\dot{E}_x^{biom} = \dot{m}_{biom}\, e_{x,biom}^{ch}. \tag{22}$$

The overall exergy output is given by the mechanical actual power output $\dot{W}_{act}$ that is the sum of the mechanical power output of the EFGT and ORC:

$$\dot{W}_{act} = \dot{W}_{EFGT} + \dot{W}_{ORC}. \tag{23}$$

The subscript "*act*" recalls that the quantity is referred to the actual irreversible process to be distinguished from the ideal reversible process. As usual, in the present exergy analysis, friction and electric losses will not be considered as they are not involved in the thermodynamic conversion process. Therefore, it is possible to define the second law efficiency from:

$$\eta_{II} = \frac{\dot{W}_{act}}{\dot{W}_{rev}}, \tag{24}$$

where:

$$\dot{W}_{rev} = \dot{E}_x^{biom} + \dot{E}_x^{rad}, \tag{25}$$

is the reversible power output that could be ideally produced in a totally reversible process. The difference between $\dot{W}_{rev}$ and $\dot{W}_{act}$ is due to the sum of the irreversibility rate or destroyed exergy in the M plant components:

Please cite this article in press as: A.M. Pantaleo, et al., Hybrid solar-biomass combined Brayton/organic Rankine-cycle plants integrated with thermal storage: Techno-economic feasibility in selected Mediterranean areas, Renewable Energy (2018), https://doi.org/10.1016/j.renene.2018.08.022

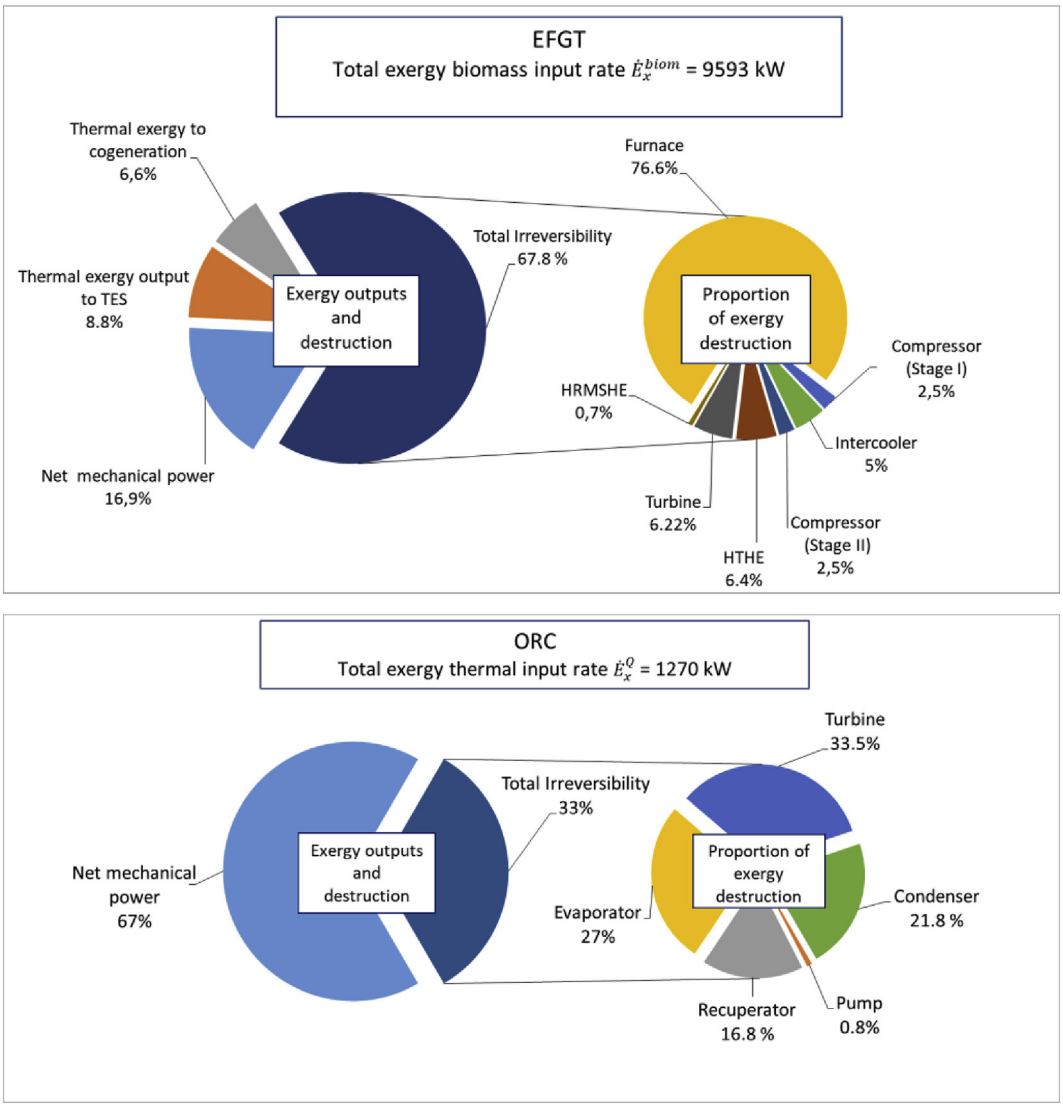

Fig. 6. Exergy balances at design point in the EFGT (top) and ORC (bottom).

$$\dot{W}_{rev} - \dot{W}_{act} = \dot{I}_{TOT} = \sum_{k=1}^{M} \dot{I}_k. \tag{26}$$

The analysis of the irreversibility rate $\dot{I}_k$in the k component, allows one to identify the root causes that originate the reduction of the actual work rate with respect to the reversible work rate.

The exergy analysis results are summarized in Table 4 and, by applying Eq. (25), it is possible to evaluate the second law efficiency of the whole system that is equal to $\eta_{II,ORC} = 0.37$. The main source of actual work reduction in the whole configuration is the EFGT whose irreversibility is 87% of the total exergy losses. At the same time, Fig. 6(a) and (b) show exergy output and destruction in the EFGT and ORC section, respectively. In particular, pie graphs on the left-hand side show exergy output and irreversibility referred to the exergy input, while the right-hand side pie chart show exergy destruction proportion caused by each component of the cycle. The second law efficiency for the main subsystems results equal to $\eta_{II,EFGT} = 0.35$ for EFGT section and $\eta_{II,ORC} = 0.67$ for the ORC. In Fig. 6(a) is it possible to see that the low value of the second low efficiency for the EFGT depends mainly on the biomass exergy input wasted in the furnace which accounts 77% of the total irreversibility, mainly due to the low temperature of the compressed air flowing in the HTHE and the exergy losses with the exhaust gas. On the other hand, ORC can convert most of the thermal input exergy in mechanical power and only the 33% is lost in irreversibility. The main sources of irreversibility in the ORC are the turbine and the evaporator that are respectively equal to 33.5% and 27% of the total losses. Very low is the exergy destruction due the heat exchange with the molten salt circuit of the TES, due to the choice of the scheme with “direct heat exchange” in which molten salts act as heat transfer fluid and heat storage medium.

4. Annual energy analysis

The analysis of the yearly electricity generated by the solar/biomass hybrid system has been carried out, considering different values of SM and TES capacities. In order to analyse the influence of the annual solar radiation on the annual energy plant production, three different locations in Fig. 7(a) have been selected.

- Case P:Priolo Gargallo (Siracusa, Italy, Latitude 37°08′04″ N, Longitude 15°03′00″E, 30 m a.s.l.);

Please cite this article in press as: A.M. Pantaleo, et al., Hybrid solar-biomass combined Brayton/organic Rankine-cycle plants integrated with thermal storage: Techno-economic feasibility in selected Mediterranean areas, Renewable Energy (2018), https://doi.org/10.1016/j.renene.2018.08.022

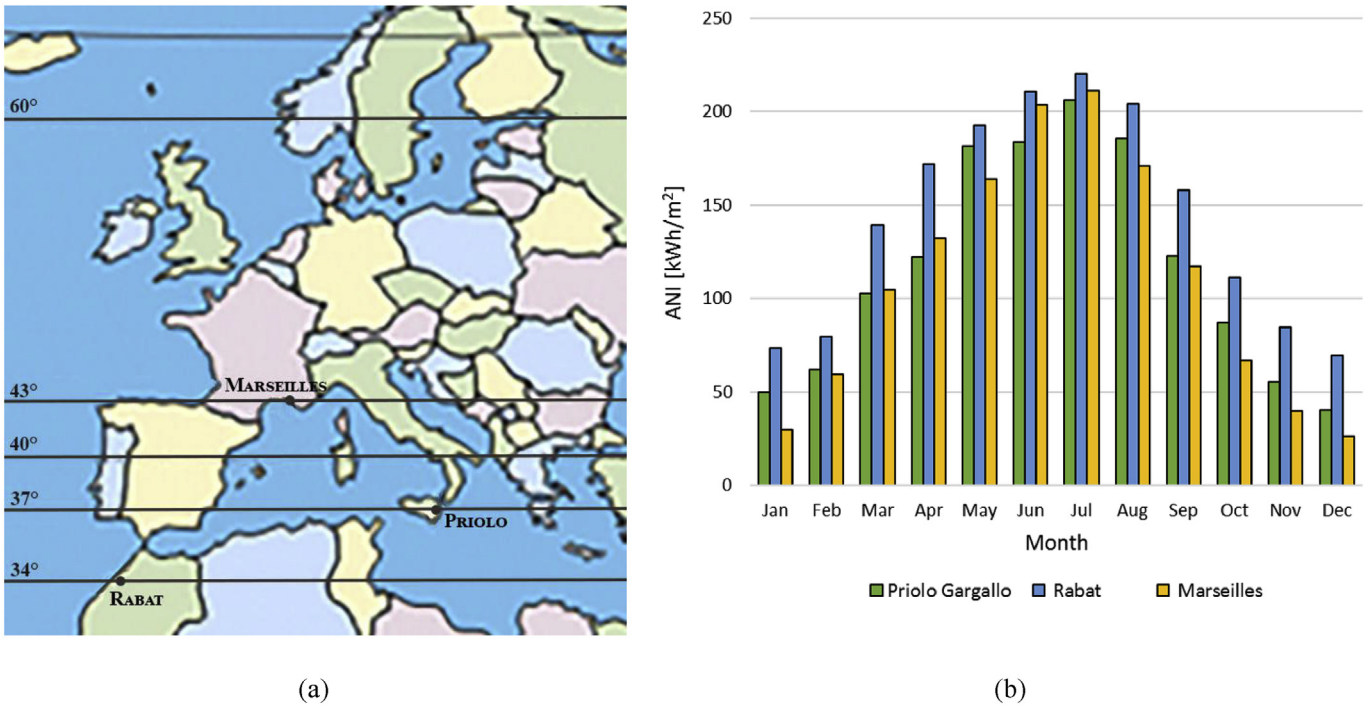

Fig. 7. (a) Site map from METEONORM [61]. (b) Monthly ANI for each site [62].

- Case M: Marseilles (France, Latitude 43°17′49″ N, Longitude 5°22′51″ E, 28 m a.s.l.);
- Case R: Rabat (Morocco, Latitude 34°00′47″ N, Longitude 6°49′57″ W, 46 m a.s.l.);

The DNI for each site has been evaluated by means of the software Meteonorm that provides accurate and representative solar radiation for any location on earth, using satellite data [61] has been carried out. The methodology proposed in Ref. [62] has been adopted to estimate the reduction coefficient of the direct normal irradiance DNI (kWh/m^2 month) and aperture normal irradiance (ANI) (kWh/m2 month) in Fig. 7(b).

The cases studies under investigation are reported in Table 5.

An hourly basis simulation on the solar field productivity has been carried out to analyse the energy performance of the system. A minimum DNI of 200 W/m2 have been considered as operational limit.

The TES capacity has been expressed in hours t_s given by the ratio of the maximum energy that can be stored E_{TES_MAX} to the solar contribution to the thermal input of the ORC, $\dot{Q}_{th,sol,ORC\_PB}$ which is set to 900 kW:

$$t_s = \frac{E_{TESMAX}}{\dot{Q}_{th,sol,ORC\_PB}} \quad (27)$$

The thermal losses are neglected (adiabatic system) and when the thermal storage is full, the excess energy is dissipated. For each location, both the solar field with SM = 2.1 and that one with SM = 4.2 (1 and 2 lines of collectors) have been considered.

Table 5
Acronyms of the examined cases.

Solar Multiple (SM)	Priolo	Marseilles	Rabat
2.1	P1	M1	R1
4.2	P2	M2	R2

Fig. 8 reports the time plot of the solar energy output, the quantity delivered to the ORC, to the TES and dissipated, for the 21st of June, in the case R1 for a TES capacity t_s = 2 h (i.e., E_{TES_MAX} = 1800 kWh). When the thermal power produced by the solar field is higher than the max thermal energy to be supplied to the ORC plant, the energy excess is delivered to the TES. If the stored energy reaches the maximum (1800 kWh), the excess of energy is dissipated. During the night, when solar energy falls down, the stored thermal energy is supplied to the ORC plant.

The Annual Energy Production (AEP) is calculated assuming a baseload operation of 8040 h per year for the biomass EFGT and for the bottoming ORC, and the solar energy production is evaluated on the basis of the TES capacity and the value of SM of the solar field. The electricity production is expressed in terms of equivalent operating hours:

$$h_{eq} = \frac{AEP}{\dot{W}_{el,tot}}. \quad (28)$$

The effect of the TES capacity on the equivalent operating hours is shown in Fig. 9 while Fig. 10 reports the amount of the solar energy dissipated in a year. As expected, the higher is the TES capacity the higher are the equivalent operating hours. On the other hand, the dissipated solar energy decreases when TES capacity increases. In Scenario 1, there is no dissipation of solar energy when the TES has a capacity higher than 12 h while in Scenario 2 the amount of dissipated solar energy increases to 5–10% according to the location. Fig. 11 reports the percentage of electricity produced by the ORC section as a percentage of the total electricity produced in a year.

The influence of the TES capacity on the annual electricity generation is reported in Fig. 12. In the scenario of single collector line (SM of 2.1), increasing the TES capacity from 6 to 8 h has a limited effect on the produced electric energy, with an increase lower than 5%, while for TES capacity higher than 12 h the further

Please cite this article in press as: A.M. Pantaleo, et al., Hybrid solar-biomass combined Brayton/organic Rankine-cycle plants integrated with thermal storage: Techno-economic feasibility in selected Mediterranean areas, Renewable Energy (2018), https://doi.org/10.1016/j.renene.2018.08.022

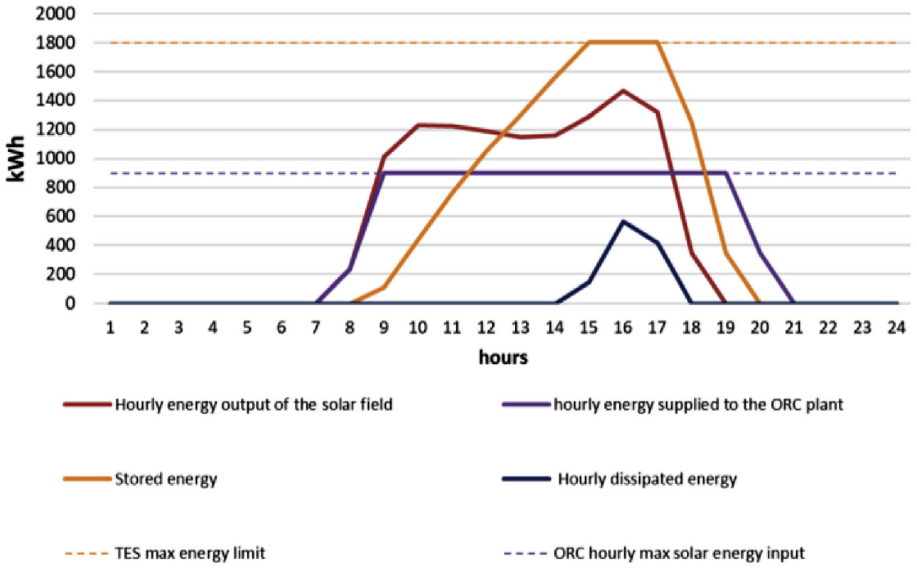

Fig. 8. Energy performance of the solar plant connected to the TES for 21st June.

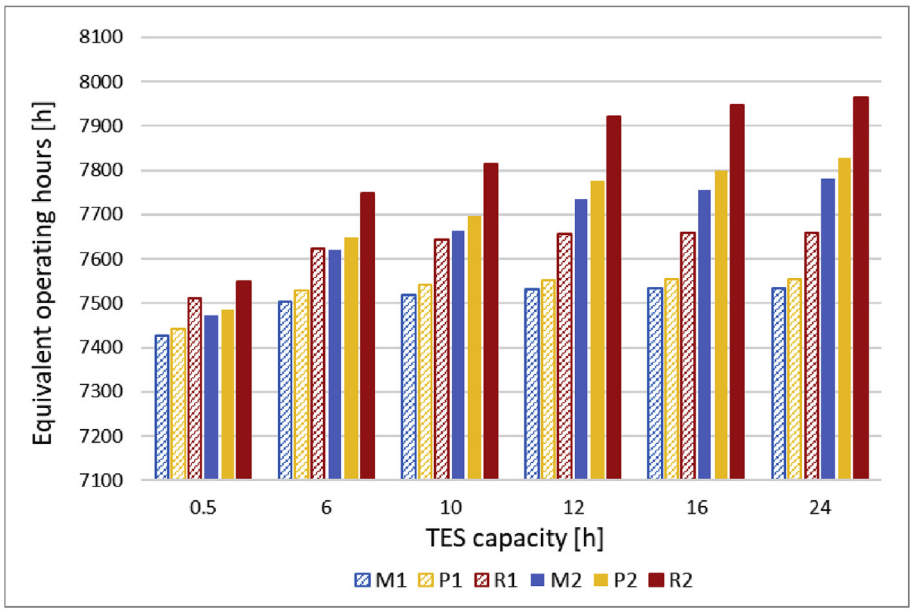

Fig. 9. Equivalent operating hours of the solar section at different TES capacity.

electric energy production is negligible, as from Fig. 12. In the case of 2 collector lines, the influence of TES capacity on the generated electricity is similar and, as also shown in Fig. 12, the advantage of a TES with a capacity higher than 12 h is negligible.

5. Cost analysis and economic assumptions

The cost analysis has been carried out assuming investment cost data from manufacturers and interviews to operators, as described in Ref. [42]. In particular, the costs of the biomass furnace have been taken from Uniconfort (Global biomass boilers) [63], the EFGT from Solar Turbines (Saturn 20) [64], the PTC from the pilot Archimede CSP plant [65] and TES [66] and from literature [67–70].

The component cost of the bottoming ORC plant has been estimated according to correlations in Seider et al. [71]:

$$C = (F) \cdot exp\left\{C_0 + C_1 \cdot \ln(S) + C_2 \cdot [\ln(S)]^2\right\} \quad (29)$$

where S is the size factor for each component and C_0, C_1, C_2 are the cost coefficients. The value used in the equation are listed in Table 6. The obtained cost figures for the ORC are compared with data from Turboden [72].

For the CSP section, the PTCs and TES costs are derived from NREL cost figures [73], according to the lessons learnt from ENEA/Enel Archimede project [65]. Unitary PTC costs of 250 Eur/m^2 and TES costs of 40 kEur/MWh are assumed. The annual operation and maintenance (O&M) costs are assumed 3.5% of the turnkey cost. In all scenarios, the biomass cost (wood chip) is 50 Eur/t at 40% moisture content and a LHV of 2.8 kWh/kg. This relatively low cost of wood chips in comparison to market price figures of 80–120 Eur/

Please cite this article in press as: A.M. Pantaleo, et al., Hybrid solar-biomass combined Brayton/organic Rankine-cycle plants integrated with thermal storage: Techno-economic feasibility in selected Mediterranean areas, Renewable Energy (2018), https://doi.org/10.1016/j.renene.2018.08.022

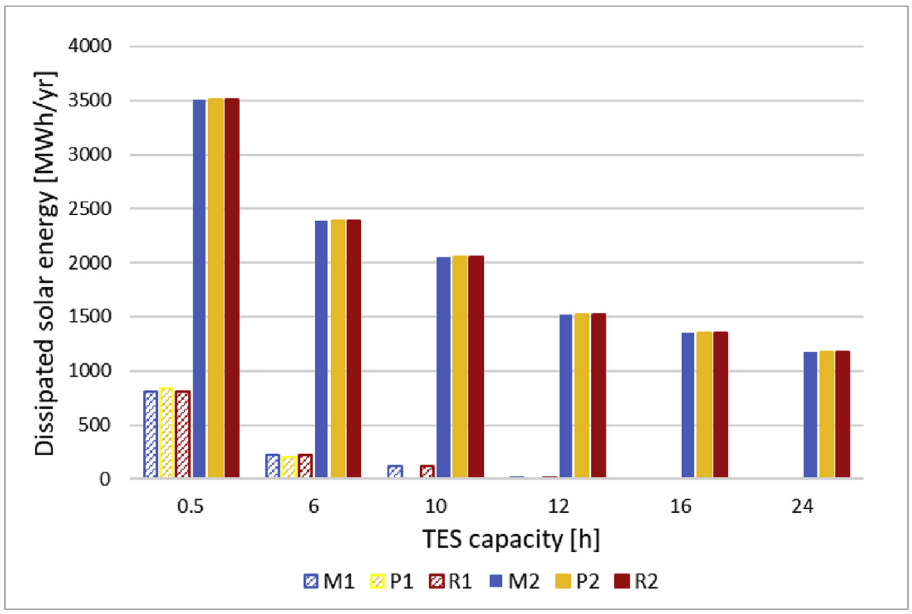

Fig. 10. Amount of dissipated solar energy in a year at different TES capacity.

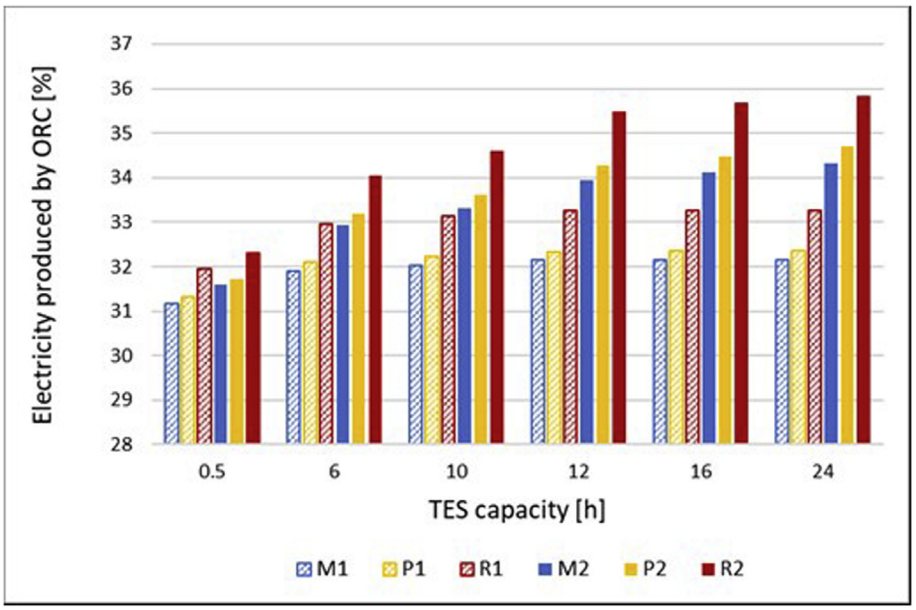

Fig. 11. Percentage of electricity produced by the ORC section respect to the total annual electricity produced by the system, at different TES capacity.

t reflects the fact that high moisture content biomass locally produced and with a low collection radius is here considered, to be dried via high temperature heat discharged by the cogeneration plant, following the assumptions in Refs. [25,35,36]. The ash discharge costs are accounted for assuming unitary cost of 70 Eur/t ash. Personnel costs are taken as 268 kEur/yr [42].

The TES cost depends on its capacity, and in Table 7 the cost figures of the optimal TES capacity of 6 and 12 h respectively for scenarios 1 and 2 are assumed as described in the next section.

From Table 7, the total predicted turnkey cost is the lowest (4.7 MEur) for the biomass-only plant (first column) that does not have a solar field, and is the highest (6.7 MEur) for scenario 2, with the largest TES and SM of 4.2. The upfront specific costs (in kEur/kWe) range between 2.3 kEur/kWe for the biomass-only plant to 3.1 kEur/kWe for the hybrid plant of scenario 2. The Opex varies from 2.28 MEur/yr for the biomass-only plant to 2.35 MEur/yr for the hybrid plant of scenario 2, in consideration of the O&M costs for the solar section.

The levelized cost of electricity (LCE) is calculated from:

$$LCE = \frac{f_a \cdot (I_{EFGT} + I_{CSP} + I_{TES} + I_{ORC} + I_{EBI}) + C_{O\&M} + C_B}{E_G}, \quad (30)$$

where f_a is the annuity factor given by:

$$f_a = \frac{r}{1 - \left(\frac{1}{1+r}\right)^l}, \quad (31)$$

and r is the discount rate, i the economic lifetime (years).

Please cite this article in press as: A.M. Pantaleo, et al., Hybrid solar-biomass combined Brayton/organic Rankine-cycle plants integrated with thermal storage: Techno-economic feasibility in selected Mediterranean areas, Renewable Energy (2018), https://doi.org/10.1016/j.renene.2018.08.022

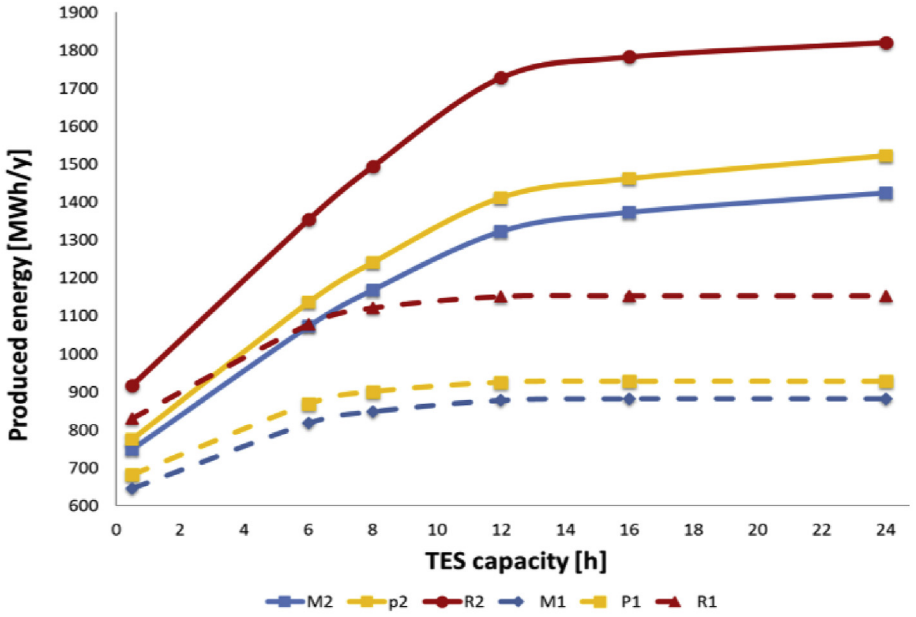

Fig. 12. Annual electricity produced by the ORC with solar input as function of TES capacity.

Table 6
Component factors used in Eq. (26).

Component	F	S	C_0	C_1	C_2
Pump	2.7	$\dot{V}\sqrt{H}$($m^3s^{-1}m^{1/2}$)	9.0073	0.4636	0.0519
Turbine	1.0	$\dot{W}_t$ (kW)	6.5106	0.8100	0
Heaters/Cooler	1.0	HTA (m^2)	10.106	−0.4429	0.0901
Evaporator/Condenser	1.0	HTA (m^2)	9.5638	0.5320	−0.0002

The financial appraisal of the investment is carried out assuming the following hypotheses: (i) 20 years of operating life and 20 years duration of the subsidy for renewable electricity in the form of feed in tariff (FiT); no 're-powering' throughout the 20 years; zero decommissioning costs, straight line depreciation of capital costs over 20 years; (ii) maintenance costs, fuel supply costs, electricity and heat selling prices held constant (in real 2018 values); (iii) cost of capital (net of inflation) equal to 5%, corporation tax neglected, no capital investments subsidies. In order to compare the investment profitability in different location, the electricity sales revenues are calculated assuming the Italian subsidy framework. This is due to the fact that there are no specific support mechanisms for such hybrid solar-bi CHP systems in France and Morocco. In the latter case, some capital grant support mechanisms could be available, according to energy policy scenarios or specific CSP projects in development [74], while in the case of France there are some feed in tariffs for biomass or solar installations which however do not specifically address hybrid configurations and concentrating solar power [75]. With these assumptions, the electricity is sold to the grid at the feed-in electricity price available in the Italian energy market for the whole plant lifetime [68], which is 180 and 296 Eur/MWh respectively for biomass electricity (assuming the use of lignocellulosic by-products in the form of wood chips from forestry harvesting) and CSP electricity [68]. These figures are valid in the considered power size range, TES size, adoption of best available technologies for emission abatement, and use of agricultural by-products from local and sustainable supply chains. The same assumptions were made for the other two locations, with the aim to assess the influence of different solar radiation on economic performance. A sensitivity analysis to the feed in tariff has been included to assess the influence of subsidies on investment profitability. The further revenues from sales of cogenerated heat at high temperature (1890 kWt at 220 °C) are included in a specific sensitivity analysis, that reports the financial profitability variation at different share of cogenerated heat sales to match local thermal energy demand, and when varying the heating selling price. The cogeneration option represents a significant increase of revenue in case of high temperature heat demand availability. The Net present value (NPV) and the Internal Rate of Return (IRR) are the economic indices assumed to appreciate the investment profitability. The NPV is calculated from Eq. (32), being $(CFi)_{dis}$ the discounted cash flow in year l, and I is the total turnkey cost:

Table 7
Capex and Opex costs. Optimized TES capacity is assumed.

Case study	Only biomass	Scenario no. 1	Scenario no. 2
Turn-key cost (kEur) I	4700	5740	6780
- Biomass EFGT section I_{EFGT}	2800	2800	2800
- CSP section I_{CSP}	–	807	1614
- TES section I_{TES}	–	216	432
- Bottoming ORC I_{ORC}	1200	1200	1200
- Engineering, building and installation I_{EBI}	700	700	700
Specific upfront cost (kEur/kWe)	2.26	2.63	3.1
O&M costs $C_{O\&M}$ (kEur/y)	487	520	523
Biomass cost C_B (kEur/y)	1285	1285	1285
Total Opex (kEur/yr)	2285	2263	2350

$$NPV = \sum_{i=1}^{l} (CF_i)_{dis} - I. \quad (32)$$

6. Techno-economic results

6.1. Levelized cost of energy and sensitivity to TES capacity

The TES capacity for each site has been selected in order to minimize the LCE, which is reported in Fig. 13. The LCE reaches its

Please cite this article in press as: A.M. Pantaleo, et al., Hybrid solar-biomass combined Brayton/organic Rankine-cycle plants integrated with thermal storage: Techno-economic feasibility in selected Mediterranean areas, Renewable Energy (2018), https://doi.org/10.1016/j.renene.2018.08.022

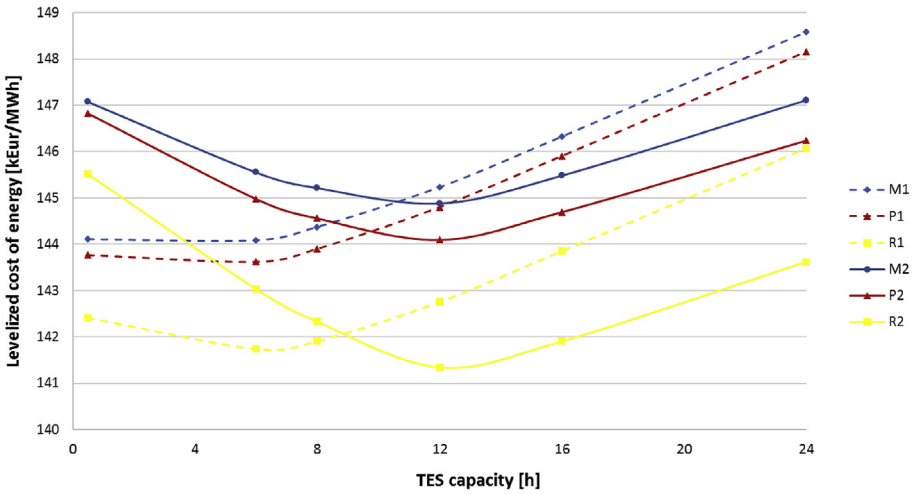

Fig. 13. LCE as function of the TES capacity for the three locations and two solar-field sizes (see acronyms in Table 2).

minimum value for a TES capacity of 6 h and 12 h respectively for the single and double collectors line scenarios. This is due to the trade-offs between the higher investment costs and higher production rate of the increased thermal storage size.

6.2. Energy performance and profitability analysis results

The energy performance analysis and the profitability assessment have been performed cassuming a TES with a capacity respectively of 6 and 12 h for the scenarios with 1 and 2 lines of collectors, which minimizes the LCE. The results are compared to those ones of a plant with 100% biomass fuel already examined in Ref. [42] and to the different hybrid configuration analysed in Ref. [43], which assumes the location of Priolo Gargallo for the solar resource analysis (cases B and C of Figs. 14 and 15, respectively with 8600 and 12,900 m^2 PTC area). In this case, the solar input from the same typology of PTCs and TES is provided to the topping gas turbine at 550 °C, so reducing the biomass consumption, but with a PTC size about 2 times larger than in the configuration here proposed. This justifies the higher LCE of the configuration of Ref. [43], despite of the higher global electric efficiency (due to the higher solar share). The global electric efficiency and the solar share at different locations and SM are reported in Fig. 14. The solar share represents the ratio of energy input from solar resource vs the total energy input to the system. Fig. 15 reports the LCE for the proposed case studies, and a comparison with the hybrid solar-biomass system configuration of Ref. [43].

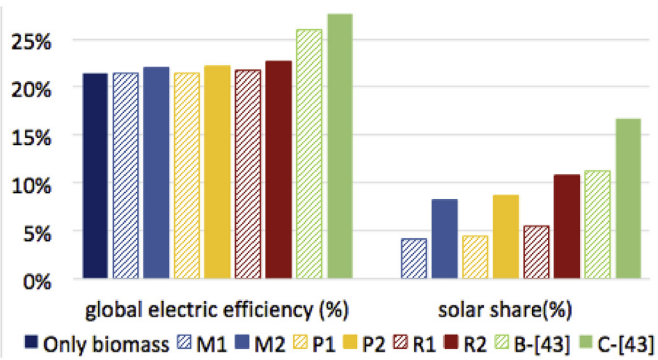

Fig. 14. Energy performance results and solar share for the different scenarios. Cases B and C represent the system configuration proposed in Ref. [43] with small and large PTC and TES size respectively.

For each case study, a sensitivity analysis to the biomass purchase price is considered. A baseload operation strategy is assumed to estimate the annual electric output. This is the best operation strategy in light of the feed-in tariffs (FiT) available for renewable CHP plants in the Italian energy market. The NPV and IRR of the investment when varying the biomass supply costs are reported in Fig. 16.

The proposed hybridization of the biomass EFGT with CSP presents higher global electric efficiency (in comparison to only biomass case), due to the solar energy input, in particular at higher SM level. As can be seen from Fig. 15, LCE values are lower than in [43], and the this is due to the lower solar section size and costs, that balance the reduced conversion efficiency on respect to the configuration [43]. Rabat is the location with the lowest LCE, due to the highest solar energy radiation and system producibility. However, all hybrid configurations present LCE higher than the one of only biomass fuel, demonstrating that the proposed CSP hybridization needs specific subsidies to be competitive with other renewable energy sources. For the only biomass scenario, LCE values range between 100 and 170 Eur/MWh at different biomass fuel costs, while for the best location of Rabat these values range between 110 and 174 Eur/MWh.

NPV ranges between 14,000 kEur (Rabat at high solar field size) to −600 kEur (Marseille with low solar field size) and IRR values from 25% (Rabat at low solar field size) down to 3.7% (Marseille at low solar field size). The hybridization of the biomass EFGT with CSP increases the global electricity efficiency, due to the solar energy input, but reduces both NPV and IRR in all the scenarios. In fact, despite the increased global energy efficiency of the solar input, and the higher electricity selling price of the solar based fraction on respect to biomass based one, the current investment costs of the PTCs with MSs as HTF are very high and make this investment not competitive. This is more evident at higher solar shares where the larger PTC solar-array areas (and consequently higher investment costs) reduce the IRR but not the NPV.

In general, the results indicate the reduced IRR of CSP integration into biomass plants, due to the high investment costs of the former, which are not compensated by the higher global energy conversion efficiency and additional electricity sale revenues. However, these results are not completely reflected in the NPV which is higher that the biomass-only case at the location of Rabat and the larger solar field (R2 of Fig. 16-a). Moreover, for biomass

Please cite this article in press as: A.M. Pantaleo, et al., Hybrid solar-biomass combined Brayton/organic Rankine-cycle plants integrated with thermal storage: Techno-economic feasibility in selected Mediterranean areas, Renewable Energy (2018), https://doi.org/10.1016/j.renene.2018.08.022

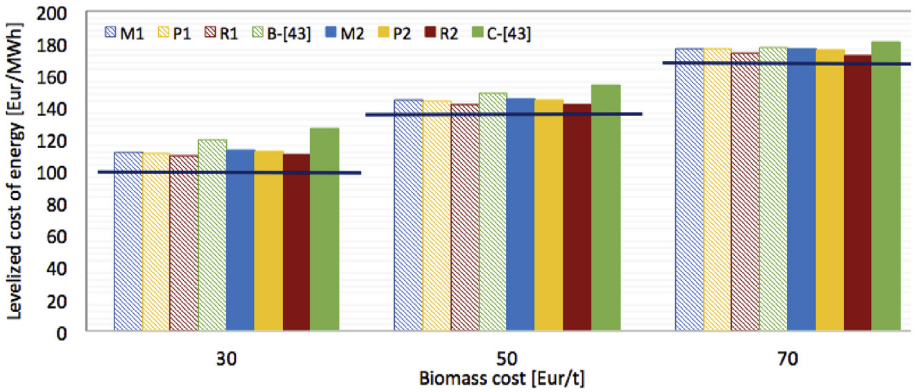

Fig. 15. LCE as function of biomass cost. Cases B and C represent the system configuration proposed in Ref. [43] with small and large PTC and TES size. The black horizontal line represents the scenario of only biomass EFGT + ORC [43].

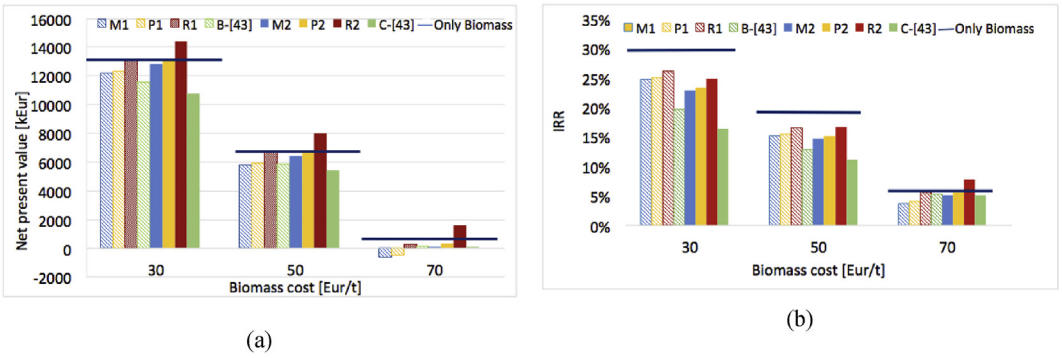

Fig. 16. (a) NPV and (b) IRR as a function of biomass supply cost for the different scenarios, and including the results of configuration [43] at small and large solar field sizing (B and C) and of configuration [42] with only biomass section.

cost of 50 Eur/t or lower, the NPV and IRR of the system configuration here proposed result higher than the correspondent values of Ref. [43]. On the other hand, for a biomass cost of 70 Eur/t the plant configuration in locations as Marseilles or Priolo Gargallo present negative NPV, except for the two collectors line scenario. Finally, the LCE and investment profitability is highly influenced by the biomass cost, and at values higher than 70 Eur/t (which are expected if no fuel source is available at low cost close to the premises of the plant) the difference between performance of only-biomass and hybrid systems decreases remarkably. In conclusion, solar hybridization of biomass CHP could be an interesting option in case of suitable feed in prices for solar based electricity generation, relatively high costs of biomass fuel supply and perspectives of cost reduction for CSP capital costs.

In Fig. 17, a sensitivity analysis of IRR and NPV to the variation of electricity feed in price is reported. Feed in prices of 20% lower than the baseline correspond to average electricity costs for industrial or large commercial consumers (150 Eur/MWh) in Italy, included generation, transmission, measurement and dispatchment costs. This scenario corresponds to on site power generation to match local electricity demand with revenues achieved as avoided electricity purchase. As can be seen, this scenario is not profitable with the assumed investment costs and in light of the expected conversion efficiencies. A different result would be achieved when

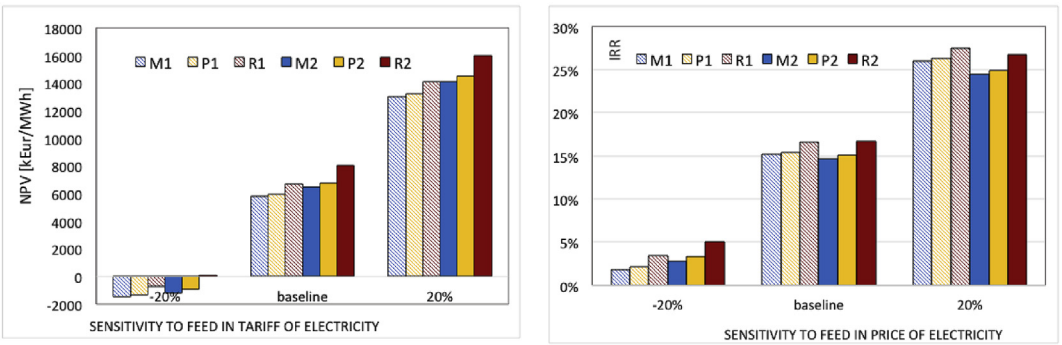

Fig. 17. Sensitivity of NPV (a) and IRR (b) to the feed-in tariff.

Please cite this article in press as: A.M. Pantaleo, et al., Hybrid solar-biomass combined Brayton/organic Rankine-cycle plants integrated with thermal storage: Techno-economic feasibility in selected Mediterranean areas, Renewable Energy (2018), https://doi.org/10.1016/j.renene.2018.08.022

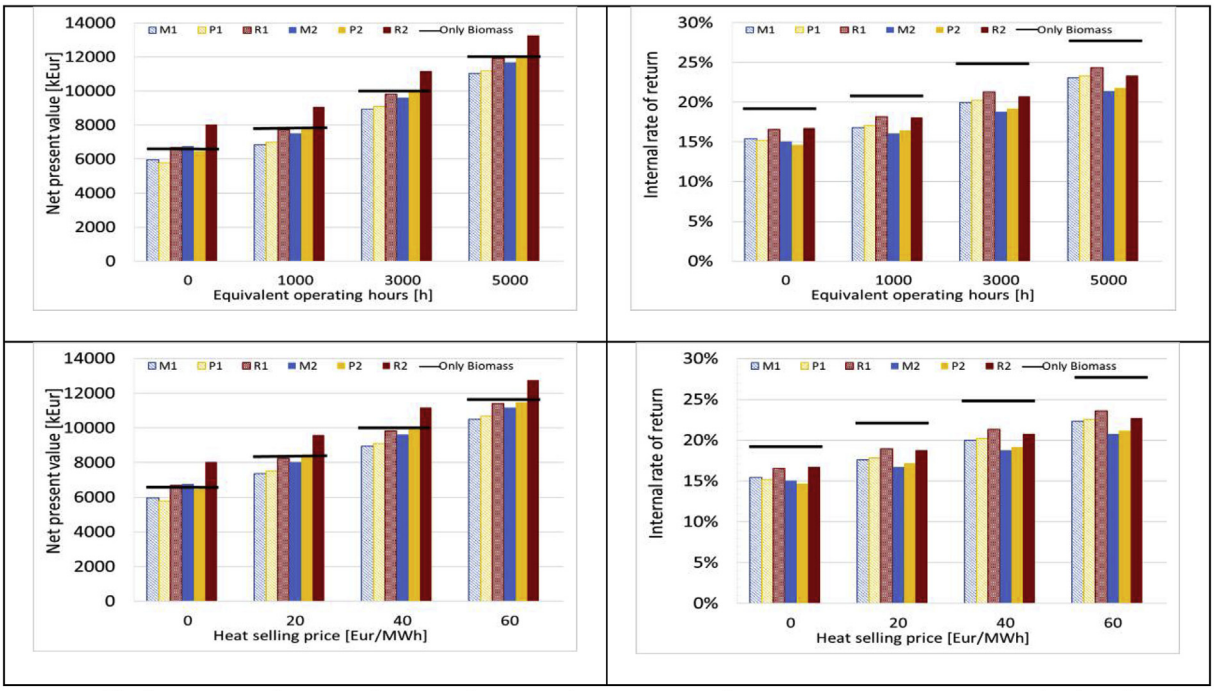

Fig. 18. Sensitivity of NPV (left) and IRR (right) to the equivalent operating hours in cogeneration option (top) and to the heating selling price (down).

using the cogenerated heat at medium-high temperature to match on site energy demand. In this case, the further revenues from thermal energy sales increase the investment profitability, as reported in Fig. 18, and this is in agreement with the results proposed in Refs. [37,43] for similar configurations. In particular, Fig. 18 reports the NPV and IRR when using the discharged heat from the plant (2100 kWt at 200 °C) to match heating demand (hot water at 70–90 °C) and with the assumption to sell the thermal energy at 40 Eur/MWh (top graphs, variation of equivalent operating hours in cogeneration mode in the range 0–5000 h/year) or to have 3000 equivalent hours/year in CHP mode operation (down graphs, variation of thermal energy selling price from 0 to 60 Eur/MWh).

7. Conclusions

A thermodynamic and economic analysis has been performed on a hybrid (solar-biomass) combined-cycle system composed of an externally fired gas-turbine (EFGT) fuelled by biomass (wood chips) and a bottoming organic Rankine cycle (ORC) plant. In order to improve the system flexibility, heat is recovered from the exhaust gases of the EFGT via a thermal energy storage (TES), which receives heat also from a field of linear parabolic-trough collectors (PTCs) with molten salts as the heat-transfer fluid (HTF). Heat from the TES is transferred to the ORC plant and to the thermal end-users, according to the heating demand profile. The thermal input to the EFGT is 9 MW, with a power output of 1.3 MW, while the ORC plant has an electric output of 700 or 800 kW with or without the solar hybridization configuration. The thermodynamic modelling was performed assuming two CSP sizes, and consequently two TES sizes. The energy performance results report higher global conversion efficiencies when using CSP integration and the thermo-economic analysis reports a higher investment NPV when integrating solar energy, due to the increased electricity generation and higher solar-based electricity selling price. A comparison with a previously proposed solar-biomass hybrid solution with a higher temperature (550 °C) of the CSP working fluid and direct solar energy input to the topping EFGT demonstrates a higher profitability of the system configuration here proposed. Another advantage of this configuration is the availability of high-grade heat for cogeneration from the bottoming ORC plant that can improve the profitability of the overall system when a suitable heat demand is available, as reported in the sensitivity analysis. The future steps of this research will focus on the quantification of the techno-economic advantages of the proposed system configuration in terms of higher generation flexibility and implementation of demand response strategies. In particular, a more detailed analysis should include specific simulation of thermal and electrical load-following operating modes for the hybrid CHP system, in order to match specific energy-demand profiles. Moreover, a key research question arises from the need to assess off-design operation, part-load and dynamic performance of the system components (EFGT, CSP and ORC) and of the whole-system. Finally, a systematic procedure for the optimization of the size of the various components on the basis of key techno-economic factors such as solar irradiance and collector efficiency, biomass availability and supply costs, time of use electricity prices and energy demand profiles would be useful to support investment decisions in the future energy systems.

Acknowledgements

This work was supported by the UK Engineering and Physical Sciences Research Council (EPSRC) [grant number EP/P004709/1] and by the Department for International Development (DFID) through the Royal Society-DFID Africa Capacity Building Initiative. The support of ENEA, Department of Energy Technologies, Division DTE-BBC, who funded the fellowship of Arianna Sorrentino in the field of “Development of biomass uses for distributed heat and power generation” is also kindly acknowledged. Data supporting this publication can be obtained on request from cep-lab@imperial.ac.uk. The authors would like to thank the Organizing Committee of the 4th International Seminar on ORC Power Systems ORC2017 (13-

15 September 2017, Milan, Italy) for awarding this paper the Best Paper Award presented at ORC2017.

References

[1] European Commission web site: https://ec.europa.eu/energy/en/topics/energy-strategy-and-energy-union/2030-energy-strategy (accessed 26-1-2018).
[2] R.P. Merchána, M.J. Santosb, A. Medinac, A. Calvo Hernándezd, Multi-stage configurations for central receiver hybrid gas-turbine thermosolar plants, in: Proceedings of ECOS, 2018.
[3] B. Coelho, A. Oliveira, P. Schwarzbözl, A. Mendes, Biomass and central receiver system (CRS) hybridization: integration of syngas/biogas on the atmospheric air volumetric CRS heat recovery steam generator duct burner, Renew. Energy 75 (2015) 665–674.
[4] J.D. Nixon, P.K. Dey, P.A. Davies, The feasibility of hybrid solar-biomass power plants in India, Energy (2012) 541–554. October.
[5] C.M.I. Hussain, B. Norton, A. Duffy, Technological assessment of different solar-biomass systems for hybrid power generation in Europe, Renew. Sustain. Energy Rev. (2016).
[6] G. San Miguel, B. Corona, Hybridizing concentrated solar power (CSP) with biogas and biomethane as an alternative to natural gas: analysis of environmental performance using LCA, Renew. Energy 66 (2014) 580–587.
[7] A. Mishra, N. Chakravarty, N. Kaushika, Thermal optimization of solar biomass hybrid cogeneration plants, J. Sci. Ind. Res. 65 (4) (2006) 355–363.
[8] M. Liu, N.H. Tay, S. Bell, M. Belusko, R. Jacob, G. Will, W. Saman, F. Bruno, Review on concentrating solar power plants and new developments in high temperature thermal energy storage technologies, Renew. Sustain. Energy Rev. 53 (2016) 1411–1432.
[9] Y. Takahisa, F. Tomohiko, A. Norio, M. Koichi, Design and testing of the organic Rankine cycle, Energy (March 2001) 239–251.
[10] M. Uris, J.I. Linares, E. Arenas, Techno-economic feasibility assessment of a biomass cogeneration plant based on an Organic Rankine Cycle, Renew. Energy 66 (2014) 707–713.
[11] R. Rayegan, Y.X. Tao, A procedure to select working fluids for Solar Organic Rankine Cycles (ORCs), Renew. Energy 36 (2011) 659–670.
[12] H.D. Madhawa Hettiarachchi, G. Mihajlo, W.M. Worek, I. Yasuyuki, Optimum design criteria for an organic Rankine cycle using low temperature geothermal heat sources, Energy 32 (2007) 1698–1706.
[13] L. Gosselin, M. Tye-Gingras, F. Mathieu-Potvin, Review of utilization of genetic algorithms in heat transfer problems, Int. J. Heat Mass Tran. (2009) 2169–2218.
[14] H. Xi, M. Li, C. Xu, Y. He, Parametric optimization of regenerative organic Rankine cycle (ORC) for low grade waste heat recovery using genetic algorithm, Energy (2013) 473–482.
[15] J. Wang, Z. Yan, M. Wang, S. Ma, Y. Dai, Thermodynamic analysis and optimization of an (organic Rankine cycle) ORC using low grade heatsource, Energy 49 (2013) 356–365.
[16] M. Petrollese, J. Oyekale, V. Tola, D. Cocco, Optimal ORC configuration for the combined production of heat and power utilizing solar energy and biomass, in: Proceedings of ECOS, 2018.
[17] T. Srinivas, B.V. Reddy, Hybrid solar-biomass power plant without energy storage, Case Stud. Therm. Eng. 2 (2014) 75–81.
[18] M. Vidal, M. Martin, Optimal coupling of a biomass based polygeneration system with a concentrated solar power facility for the constant production of electricity over a year, Comput. Chem. Eng. 72 (2015) 273–283.
[19] J.H. Peterseim, S. White, A. Tadros, U. Hellwig, Concentrated solar power hybrid plants, which technologies are best suited for hybridisation? Renew. Energy 57 (2013) 520–532.
[20] J.H. Peterseim, S. White, A. Tadros, U. Hellwig, Concentrating solar power hybrid plants - enabling cost effective synergies, Renew. Energy 67 (2014) 178–185.
[21] Á. Pérez, N. Torres, Solar parabolic trough e biomass hybrid plants: a cost efficient concept suitable for places in low irradiation conditions, in: SolarPACES Conference, 2010.
[22] L. Schnatbaum, Biomass utilization for Co firing in parabolic trough power plants, in: SolarPACES Conf, 2009.
[23] V. Piemonte, M. De Falco, P. Tarquini, A. Giaconia, Life Cycle Assessment of a high temperature molten salt concentrated solar power plant, Sol. Energy 85 (5) (2011) 1101–1108, https://doi.org/10.1016/j.solener.2011.03.002.
[24] A. Amoresano, G. Langella, S. Sabino, Optimization of solar integration in biomass fuelled steam plants, Energy Proced. 81 (2015) 390–398.
[25] J.H. Peterseim, A. Tadros, S. White, U. Hellwig, F. Klostermann, Concentrated solar power/energy from waste hybrid plants e creating synergies, in: SolarPACES Conference, 2012.
[26] European Concentrated Solar Thermal Road-mapping, 2005. SES6-CT-2003-502578, DLR, http://www.promes.cnrs.fr/uploads/pdfs/ecostar/ECOSTAR.Roadmap.pdf.
[27] Z. Bai, O. Lium, J. Lei, H. Hong, H. Jin, New solar-biomass power generation system integrated a two-stage gasifier, Appl. Energy (2016). https://doi.org/10.1016/j.apenergy.2016.06.
[28] J. Soares, A.C. Oliveira, Numerical simulation of a hybrid concentrated solar power/biomass mini power plant", Appl. Therm. Eng. (2016). https://doi.org/10.1016/j.applthermaleng.2016.06.180.
[29] E.K. Burin, L. Buranello, P. Lo Giudice, T. Vogel, K. Grner, E. Bazzo, Boosting power output of a sugarcane bagasse cogeneration plant using parabolic trough collectors in a feedwater heating scheme, Appl. Energy 154 (2015) 232–241, 2015.
[30] A. Pantaleo, A. Pellerano, M.T. Carone, Potentials and feasibility assessment of small scale CHP plants fired by energy crops in Puglia region (Italy), Biosyst. Eng. 102 (3) (2009) 345–359, https://doi.org/10.1016/j.biosystemseng.2008.12.002.
[31] G. Riccio, D. Chiaramonti, Design and simulation of a small polygeneration plant cofiring biomass and natural gas in a dual combustion micro gas turbine (BIO_MGT), Biomass Bioenergy 33 (11) (2009) 1520–1531.
[32] A.M. Pantaleo, S.M. Camporeale, N. Shah, Thermo-economic assessment of externally fired micro-gas turbine fired by natural gas and biomass: applications in Italy, Energy Convers. Manag. 75 (2013) 202–213.
[33] A.M. Pantaleo, S. Camporeale, N. Shah, Natural gas–biomass dual fuelled microturbines: comparison of operating strategies in the Italian residential sector, Appl. Therm. Eng. 71 (2) (2014) 686–696.
[34] S. Camporeale, F. Turi, M. Torresi, B. Fortunato, A. Pantaleo, A. Pellerano, Part load performances and operating strategies of a natural gas-biomass dual fuelled microturbine for CHP operation, J. Eng. Gas Turbines Power 137 (12) (2015).
[35] S. Barsali, R. Giglioli, G. Ludovici, D. Poli, A micro combined cycle plant for power generation from solid biomass: Coupling EFMGT and ORC, in: 19th European Biomass Conference, ETA-WIP, Berlin, 2011.
[36] A. Bagdanavicius, R. Sansom, N. Jenkins, G. Strbac, Economic and exergoeconomic analysis of micro GT and ORC cogeneration systems, in: ECOS 2012, 2012, pp. 1–11.
[37] G. Qiu, Selection of working fluids for micro-CHP systems with ORC, Renew. Energy 48 (2012) 565–570.
[38] O.A. Oyewunmi, A.I. Taleb, A.J. Haslam, C.N. Markides, An assessment of working-fluid mixtures using SAFT-VR Mie for use in organic Rankine cycle systems for waste-heat recovery, Comput. Therm. Sci. 6 (4) (2014) 301–316, https://doi.org/10.1615/.2014011116.
[39] O.A. Oyewunmi, A.I. Taleb, A.J. Haslam, C.N. Markides, On the use of SAFT-VR Mie for assessing large-glide fluorocarbon working-fluid mixtures in organic Rankine cycles, Appl. Energy 163 (2016) 263–282, https://doi.org/10.1016/j.apenergy.2015.10.040.
[40] O.A. Oyewunmi, C.N. Markides, Thermo-economic and heat transfer optimization of working-fluid mixtures in a low-temperature organic Rankine cycle system, Energies 9 (6) (2016) 1–21, https://doi.org/10.3390/en9060448, 448.
[41] L. Pratticò, L. Toccia, E. Sciubba, Performance assessment of a solar-powered Organic Rankine Cycle for combined heat and power generation in small size rural applications, in: Proceedings of ECOS, 2018.
[42] S. Camporeale, A. Pantaleo, P. Ciliberti, B. Fortunato, Cycle configuration analysis and techno-economic sensitivity of biomass externally fired gas turbine with bottoming ORC, Energy Convers. Manag. 105 (2015) 1239–1250.
[43] A. Pantaleo, S. Camporeale, A. Miliozzi, V. Russo, C.N. Markides, N. Shah, Novel hybrid CSP-biomass CHP for flexible generation: Thermo-economic analysis and profitability assessment, Appl. Energy 204 (2017) 994–1006, https://doi.org/10.1016/j.apenergy.2017.05.019.
[44] H. Zhang, B. Jan, G. Cáceres, D. Jan, Y. Lv, Thermal energy storage: recent developments and practical aspects, Prog. Energy Combust. Sci. 53 (2016) 1–40. ISSN 0360–1285, https://doi.org/10.1016/j.pecs.2015.10.003.
[45] ENEA Working Group, Solar Thermal Energy Production: Guidelines and Future Programmes of ENEA, 2001. ENEA Report. Available at: http://www.solaritaly.enea.it/Documentazione/Documentazione.php.
[46] Technology Roadmap, Concentrating Solar Power, International Energy Agency, 2010.
[47] G.M. Giannuzzi, C.E. Majorana, A. Miliozzi, V.A.L. Salomoni, D. Nicolini, Structural design criteria for steel components of parabolic-trough solar concentrators, J. Sol. Energy Eng. 129 (2007) 382–390.
[48] V.A. Salomoni, C.E. Majorana, G.M. Giannuzzi, A. Miliozzi, D. Nicolini, in: Radu D. Rugescu (Ed.), New Trends in Designing Parabolic Trough Solar Concentrators and Heat Storage Concrete Systems in Solar Power Plants, Solar Energy, InTech, 2010. ISBN: 978-953-307-052-0.
[49] R.W. Bradshow, D.R. Meeker, High temperature stability of ternary nitrate molten salts for solar thermal energy systems, Sol. Energy Mater. (1990) 51–60.
[50] U. Herrmann, B. Kelly, H. Price, Two-tank molten salt storage for parabolic trough solar power plants, Energy 29 (5–6) (2004) 883–893.
[51] H. Hottel, B. Woertz, Thermal theory and Modeling of Solar Collectors, MIT press, Cambridge, MA, 1990.
[52] ENEA web Site: www.solaritaly.enea.it (accessed 20-12-2017).
[53] P.J. Mago, L.M. Chamra, K. Srinivasan, C. Somayaji, An examination of regenerative organic Rankine cycles using dry fluids, Appl. Therm. Energy (2008) 998–1007.
[54] R. Chacartegui, D. Sánchez, J.M. Muñoz, T. Sánchez, Alternative ORC bottoming cycles FOR combined cycle power plants, Appl. Energy (2009) 2162–2170.
[55] I.H. Bell, J. Wronski, S. Quolin, V. Lemort, Pure and pseudo-pure fluid thermophysical property evaluation and the open-source thermophysical property library CoolProp, Ind. Eng. Chem. Res. 53 (6) (2014) 2498–2508.
[56] M.J. Moran, H.N. Shapiro, D.D. Boettner, M.B. Bailey, Fundamentals of Engineering Thermodynamics, John Wiley & Sons, 2010.
[57] T.J. Kotas, The Exergy Method of Thermal Plant Analysis, Elsevier, 2013.

Please cite this article in press as: A.M. Pantaleo, et al., Hybrid solar-biomass combined Brayton/organic Rankine-cycle plants integrated with thermal storage: Techno-economic feasibility in selected Mediterranean areas, Renewable Energy (2018), https://doi.org/10.1016/j.renene.2018.08.022

[58] F. Gharagheizi, M. Mehrpooya, Prediction of standard chemical exergy by a three descriptors QSPR model, Energy Convers. Manag. 48 (2007) 2453–2460.
[59] M. Mehrpooya, M. Khalili, M. Mehdi Moftakhari Sharifzadeh, Model development and energy and exergy analysis of the biomass gasification process (Based on the various biomass sources), Renew. Sustain. Energy Rev. 91 (2018) 869–887. ISSN 1364–0321, https://doi.org/10.1016/j.rser.2018.04.076.
[60] H. Li, X. Zhang, L. Liu, R. Zeng, G. Zhang, Exergy and environmental assessments of a novel trigeneration system taking biomass and solar energy as co-feeds, Appl. Therm. Eng. 104 (2016) 697–706. ISSN 1359–4311, https://doi.org/10.1016/j.applthermaleng.2016.05.081.
[61] Web site Irradiation data: http://www.meteonorm.com.
[62] M. Sengupta, A. Habte, S. Kurtz, A. Dobos, S. Wilbert, E. Lorenz, T. Stoffel, D. Renné, C. Gueymard, D. Myers, S. Wilcox, P. Blanc, R. Perez, Best Practices Handbook for the Collection and Use of Solar Resource Data for Solar Energy Applications, February 2015. Technical Report, NREL/TP-5D00-63112.
[63] Uniconfort website: https://www.uniconfort.com (accessed 20-1-2018) and personal communications.
[64] Solar Turbines website: https://mysolar.cat.com (accessed 25-1-2018) and personal communications.
[65] Archimede solar power plant, https://en.wikipedia.org/wiki/Archimede_solar_power_plant.
[66] S. Sau, N. Corsaro, T. Crescenzi, C. D'Ottavi, R. Liberatore, S. Licoccia, V. Russo, P. Tarquini, A.C. Tizzoni, Techno-economic comparison between CSP plants presenting two different heat transfer fluids, Appl. Energy 168 (2016) 96–109.
[67] V. Russo, CSP plant thermal-hydraulic simulation, Energy Proced. 49 (2014) 1533–1542. Proceedings of the SolarPACES 2013 International Conference.
[68] Italian Ministry of Economic Development, Incentives for energy from electric not-photovoltaic renewable sources, Legislative decrees of 07.06.2016.
[69] R. Sterrer, S. Schidler, O. Schwandt, P. Franz, A. Hammerschmid, ScienceDirect Theoretical Analysis of the Combination of CSP with a Biomass CHP-plant Using ORC-technology in Central Europe, vol. 49, 2014, pp. 1218–1227. http://doi.org/10.1016/j.egypro.2014.03.131.
[70] S.S. Mostafavi Tehrani, R.A. Taylor, K. Nithyanandam, S.A. Ghazani, Annual comparative performance and cost analysis of high temperature, sensible thermal energy storage systems integrated with a concentrated solar power plant, Sol. Energy 153 (2017) 153–172.
[71] W.D. Seider, J.D. Seader, D.R. Lewin, Product & Process Design Principles: Synthesis, Analysis and Evaluation, John Wiley & Sons, Hoboken, NJ, USA, 2009.
[72] Turboden Web Site www.turboden.com and personal communications.
[73] C. Turchi, Parabolic Trough Reference Plant for Cost Modeling with the Solar Advisor Model (SAM), July 2010. Technical Report, NREL/TP-550-47605.
[74] Renewable Energy and Energy Efficiency in Morocco, Moroccan-German Energy Partnership PAREMA, 2016. Report available at: http://dkti-maroc.org/wp-content/uploads/sites/61/2016/11/PAREMA_sme-re-ee-morocco.pdf.
[75] Legal Resources on Renewable Energy web site: http://www.res-legal.eu/search-by-country/france/single/s/res-e/t/promotion/aid/feed-in-tariff-tarif-dachat/lastp/131/(accessed 26-1-2018).
[76] C.N. Markides, The role of pumped and waste heat technologies in a high-efficiency sustainable energy future for the UK, Appl. Therm. Eng. 53 (2) (2013) 197–209, https://doi.org/10.1016/j.applthermaleng.2012.02.037.
[77] C.N. Markides, Low-concentration solar-power systems based on organic Rankine cycles for distributed-scale applications: overview and further developments, Front. Energy Res. 3 (2015) 1–16, https://doi.org/10.3389/fenrg.2015.00047. Article Number 47.
[78] J. Freeman, K. Hellgardt, C.N. Markides, An assessment of solar–thermal collector designs for small-scale combined heating and power applications in the United Kingdom, Heat Transf. Eng. 36 (14-15) (2015) 1332–1347, https://doi.org/10.1080/01457632.2015.995037.
[79] O.A. Oyewunmi, C.J.W. Kirmse, A.M. Pantaleo, C.N. Markides, Performance of working-fluid mixtures in ORC-CHP systems for different heat-demand segments and heat-recovery temperature levels, Energy Convers. Manag. 148 (2017) 1508–1524, https://doi.org/10.1016/j.enconman.2017.05.078.
[80] M.A. Chatzopoulou, C.N. Markides, Thermodynamic optimisation of a high-electrical efficiency integrated internal combustion engine–organic Rankine cycle combined heat and power system, Appl. Energy 226 (2018) 1229–1251, https://doi.org/10.1016/j.apenergy.2018.06.022.
[81] J. Freeman, K. Hellgardt, C.N. Markides, An assessment of solar-powered organic Rankine cycle systems for combined heating and power in UK domestic applications, Appl. Energy 138 (2015) 605–620, https://doi.org/10.1016/j.apenergy.2014.10.035.
[82] J. Freeman, K. Hellgardt, C.N. Markides, Working fluid selection and electrical performance optimisation of a domestic solar-ORC combined heat and power system for year-round operation in the UK, Appl. Energy 186 (2017) 291–303, https://doi.org/10.1016/j.apenergy.2016.04.041.
[83] J. Freeman, I. Guarracino, S.A. Kalogirou, C.N. Markides, A small-scale solar organic Rankine cycle combined heat and power system with integrated thermal energy storage, Appl. Thermal Eng. 127 (2017) 1543–1554, https://doi.org/10.1016/j.applthermaleng.2017.07.163.
[84] A. Ramos, M.A. Chatzopoulou, J. Freeman, C.N. Markides, Optimisation of a high-efficiency solar-driven organic Rankine cycle for applications in the built environment, Appl. Energy 228 (2018) 755–765, https://doi.org/10.1016/j.apenergy.2018.06.059.
[85] M.T. White, O.A. Oyewunmi, A.J. Haslam, C.N. Markides, Industrial waste-heat recovery through integrated computer-aided working-fluid and ORC system optimisation using SAFT-γ Mie, Energy Convers. Manag. 150 (2017) 851–869, https://doi.org/10.1016/j.enconman.2017.03.048.
[86] M.T. White, O.A. Oyewunmi, M.A. Chatzopoulou, A.M. Pantaleo, A.J. Haslam, C.N. Markides, Computer-aided working-fluid design, thermodynamic optimisation and thermoeconomic assessment of ORC systems for waste-heat recovery, Energy 161 (2018) 1181–1198, https://doi.org/10.1016/j.energy.2018.07.098.
[87] O.A. Oyewunmi, S. Lecompte, M. De Paepe, C.N. Markides, Thermoeconomic analysis of recuperative sub-and transcritical organic Rankine cycle systems, Energy Proc. 129 (2017) 58–65, https://doi.org/10.1016/j.egypro.2017.09.187.

Nomenclature

Symbols

b: Availability
C: Cost
C: Velocity
CF_i: Discounted cash flow
C_p: specific heat
$\dot{E}$: Power input
E_G: Total produced electricity
$\dot{e}_x$: Exergy
F_a: Annuity factor
G: Gravitational acceleration
h: Enthalpy
I: Turnkey cost
$\dot{I}$: Irreversibility
I: Economic lifetime
$\dot{m}$: Mass flow
$\dot{W}$: Mechanical power absorbed/produced
$\dot{Q}$: Thermal power
s: Entropy
T: Temperature
x: Mole fraction
z: Geodetic height

Greek

β: Coefficient
η: Efficiency

Subscripts

I: First law
II: Second law
0: Dead state
1,2,3…: State points of the ORC
A,B,C…: State points of the EFGT
Amb: Ambient
Av: Available
Biom: Biomass
C,I: First compressor stage
C,II: Second compressor stage
Cog: Cogeneration
CSP: Concentrating solar power
EBI: Engineering building and installation
EFGT: Externally fired gas turbine
EL: Electric
Fur: Furnace
g: Gas in EFGT
gen: Generator
Int: Internal
Obt: Obtained
O&M: Operation and maintenance
ORC: Organic Rankine cycle
ORC_PB: Organic Rankine cycle power block
Rec: Recovered
Sol: Solar
T: Turbine
TES: Thermal energy storage
Th: Thermal
TIT: Turbine inlet temperature
Tot: Total

Superscripts

ph: Physical

Please cite this article in press as: A.M. Pantaleo, et al., Hybrid solar-biomass combined Brayton/organic Rankine-cycle plants integrated with thermal storage: Techno-economic feasibility in selected Mediterranean areas, Renewable Energy (2018), https://doi.org/10.1016/j.renene.2018.08.022

ch: Chemical

Abbreviations

AEP: Annual energy production
ANI: Aperture normal irradiance (normal to the aperture plane)
CHP: Combined heat and power
CSP: Concentrating solar power
DNI: Direct normal insolation (direct beam solar radiation on a plane normal to the sun's rays)
EFGT: Externally-fired gas turbine
FiT: Feed-in-tariff
GA: Genetic algorithm
GWP: Global warming potential
HRMSHE: Heat-recovery molten-salt heat exchanger
HRVG: Heat recovery vapour generation
HTF: Heat transfer fluid
HTHE: High temperature heat exchanger
IRR: Internal rate of return
LCE: Levelized cost of energy
LHV: Lower heating value
NPV: Net present value
ODP: Ozone depletion potential
PTC: Parabolic-trough collector
RHE: Recuperative heat exchanger
SCA: Solar collector assembly
SM: SOLAR MULTIPLE

Please cite this article in press as: A.M. Pantaleo, et al., Hybrid solar-biomass combined Brayton/organic Rankine-cycle plants integrated with thermal storage: Techno-economic feasibility in selected Mediterranean areas, Renewable Energy (2018), https://doi.org/10.1016/j.renene.2018.08.022